



## **STRUCTURAL SYSTEMS RESEARCH PROJECT**

Report No.  
TR-2000/4

## **PRELIMINARY EVALUATION OF THE HYBRID TUBE BRIDGE SYSTEM**

**By**

**Lei Zhao**

**Rigoberto Burgueño**

**Henriette La Rovere**

**Frieder Seible**

**Vitasp Karbhari**

Final Test Report Submitted to California Department of  
Transportation under Contract No. 59AO032

February 2000

Department of Structural Engineering  
University of California, San Diego  
La Jolla, California 92093-0085

University of California, San Diego  
Department of Structural Engineering  
Structural Systems Research Project

Report No. TR-2000/04

## **Preliminary Evaluation of the Hybrid Tube Bridge System**

By

**Lei Zhao**

Assistant Project Scientist

**Rigoberto Burgueio**

Assistant Project Scientist

**Henriette La Rovere**

Assistant Project Scientist

**Frieder Seible**

Professor of Structural Engineering

**Vistasp Karbhari**

Assistant Professor of Structural Engineering

Final Test Report Submitted to California Department of Transportation  
under Contract No. 59AO032

Department of Structural Engineering  
University of California, San Diego  
La Jolla, California 92093-0085

February 2000

# TABLE OF CONTENTS

<b>1</b>	<b>DEVELOPMENT OF MODULAR ADVANCED COMPOSITE BRIDGE SYSTEMS.....</b>	<b>1</b>
1.1	Concrete Filled Carbon Shell System (CSS).....	1
1.2	Hybrid Tube System (HTS) .....	3
1.3	Applications .....	6
1.3.1	Kings Stormwater Channel Bridge.....	6
1.3.2	I-5/Gilman advanced composite cable stayed bridge .....	10
1.4	Scope of The Report.....	16
<b>2</b>	<b>MANUFACTURING AND MATERIAL PROPERTIES OF THE COMPONENTS</b>	<b>16</b>
2.1	Materials Specifications .....	16
2.1.1	FRP composites.....	16
2.1.2	Fiber-reinforced concrete .....	17
2.2	Manufacturing of FRP Components .....	17
2.3	FRP Hybrid Girder.....	21
2.4	Shear Stirrups.....	23
2.5	Tension Tie Panels .....	23
2.6	Concrete .....	23
2.6.1	Compressive properties .....	24
2.6.2	Split-tension properties .....	24
2.6.3	Modulus of rupture.....	25
2.6.4	Summary of concrete properties.....	25
<b>3</b>	<b>FLEXURAL TEST OF A HYBRID TUBE GIRDER .....</b>	<b>26</b>
3.1	Test Setup.....	26
3.2	Test Observations.....	28
3.3	Test Results .....	29
<b>4</b>	<b>TEST OF THE HYBRID TUBE SUBASSEMBLAGE .....</b>	<b>33</b>
4.1	Assembly and Construction of HTS Two-Girder Sub-Assemblage.....	33
4.1.1	Components.....	33
4.1.2	Assembly.....	35
4.2	Flexural Test .....	39
4.2.1	Test setup .....	39
4.2.2	Instrumentation layout.....	41
4.2.3	Test observations.....	43
4.2.4	Test results .....	45
4.3	Punching Shear Test.....	51
4.3.1	Test setup .....	51
4.3.2	Test observations.....	51
4.3.3	Test results .....	53
<b>5</b>	<b>CONCLUSIONS.....</b>	<b>55</b>
<b>6</b>	<b>REFERENCES .....</b>	<b>56</b>

# 1 DEVELOPMENT OF MODULAR ADVANCED COMPOSITE BRIDGE SYSTEMS

Advanced composite materials, or fiber reinforced polymers (FRPs), have been widely used in recent years for the rehabilitation of existing structures in the form of seismic retrofit, service load strengthening, and damage repair measures. Their use to date in new structural systems has been limited to a few demonstration projects, since material and manufacturing costs are still uncertain. Clear advantages of the FRPs for civil applications such as the light weight and easy handling, low maintenance and increased durability, as well as tailorability for function and demand, can only be realized when new design concepts and structural systems offer reduced material usage and simplified construction procedures combined with reduced erection times.

Material cost issues can only be addressed by prudent use of the FRPs in design through (1) eliminating the notion of simple component replacement in the form of reinforcing bars, prestressing tendons and structural shapes, (2) development of new structural shapes and geometries which lend themselves to both function and manufacturability, (3) combining conventional materials with FRPs, and (4) development of connection concepts which can significantly simplify the on-site assembly. Only once these issues are properly addressed will cost, as a dominant factor, be competitive enough to allow durability and maintenance to be considered. For short and medium span bridges, economical bridge systems and construction technologies require even further efforts to address the above issues. Only significantly lower construction and erection times derived from light weight, modular and easy to connect components will provide material-cost offsetting benefits in the form of reduced lane closures and fewer traffic interruptions in urban areas.

To provide new bridge systems that can be cost-competitive with conventional bridge construction practice, two systems for short and medium span bridges have been under development at the University of California, San Diego. The systems combine modular, factory produced FRP components with conventional materials as well as innovative connection and assembly technologies. The first system consists of filament wound thin-walled carbon shells filled with concrete and used as bridge columns, girders and cross-beams in combination with conventional reinforced concrete (RC) bridge decks or modular pultruded fiberglass decks. The concrete filled carbon shell systems (CSS) rely on conventional civil engineering connection technologies in the form of embedded dowels or connection reinforcement and are briefly described in the next section. The second system is based on hollow pultruded hybrid tube girders or beams with modular connections and RC decks.

## 1.1 Concrete Filled Carbon Shell System (CSS)

The concrete filled carbon shell system (CSS) was developed following very successful tests on bridge columns retrofitted with thin carbon jackets to provide ductility and shear strength for seismic retrofit [1]. The high confinement achieved in seismic column retrofit with thin carbon jackets was translated to a thin walled pre-manufactured carbon shell with both hoop ( $90^\circ$  from the member axis) and longitudinal ( $\pm 10^\circ$ ) fibers produced by the wet filament winding process. A special mandrel provides helical ribs on the inside of the carbon shell to aid in the force transfer between the infill concrete and the shell, see Figure 1.1.

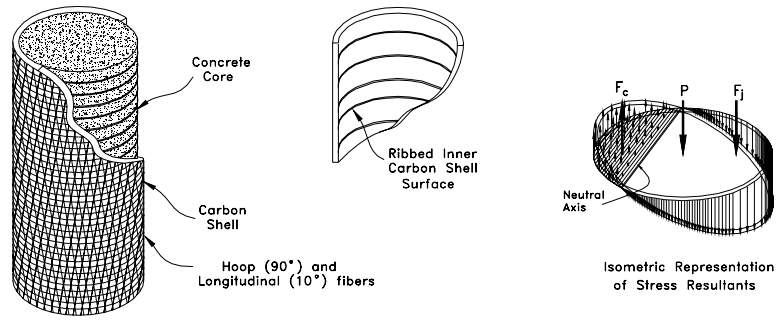


**Figure 1.1 Concrete filled carbon shell system**

The well confined concrete provides for compression force transfer as well as stabilization of the thin walled carbon shell against buckling, and the carbon shell provides the stay-in-place concrete form, the longitudinal flexural reinforcement and the hoop confinement. The concept was validated for CSS columns with large scale flexural tests that featured conventional starter bar connections, allowing displacement ductilities of  $\mu_{\Delta} = 8$  to be reached prior to starter bar rupture in low cycle fatigue. In case metallic connections are not desirable, the carbon shell can be directly embedded into the footing, resulting in a stronger yet less ductile connection concept and column response. While significant overstrength would be needed in the more linear elastic to failure FRPs to derive at an equivalent safety factor against failure in an energy sense, design comparisons have shown that most FRP component or system designs are stiffness driven and that the available material strength cannot be fully utilized in many applications.

Following the CSS column tests, the system was further developed for use as girders and beams [2]. While still very advantageous in terms of concrete confinement and for the filament winding manufacturing process, the circular cross-section has limitations in girder type applications which resulted in the development of square or rectangular thin walled carbon shells as shown in Figure 1.2. The sections with large rounded corners still exhibit significant confinement effects.

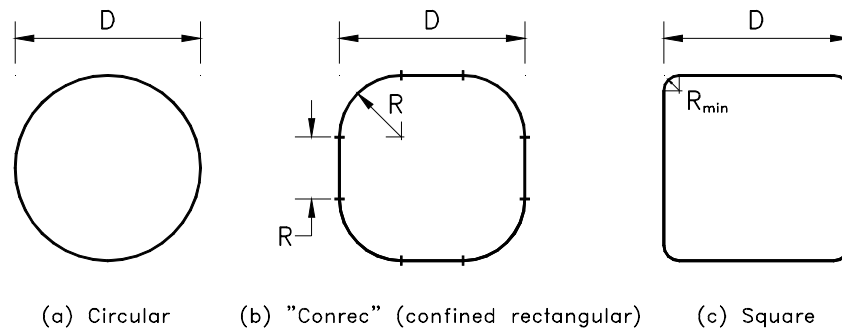


**Figure 1.2 Potential carbon shell system cross-sectional geometries**

Similar to the column end connections, girders can be spliced where necessary with either mild reinforced bars or with FRP reinforcing units. The CSS girders can be combined with a conventional RC bridge deck or a FRP modular deck system to form a complete deck system. The connection between the decks and the concrete filled carbon shells can again be accomplished with conventional dowel technology by embedding shear connectors into the shell system during grouting. In the deck the dowels are either cast directly into the RC deck or anchored in polymer concrete filled sections of the E-glass deck. The modular E-glass deck consists of pultruded trapezoidal elements bonded together and overlaid with continuous face sheets under factory system [3]. Tests conducted on such FRP decks have shown that its stiffness falls within the bounds established by the cracked and uncracked stiffness of a



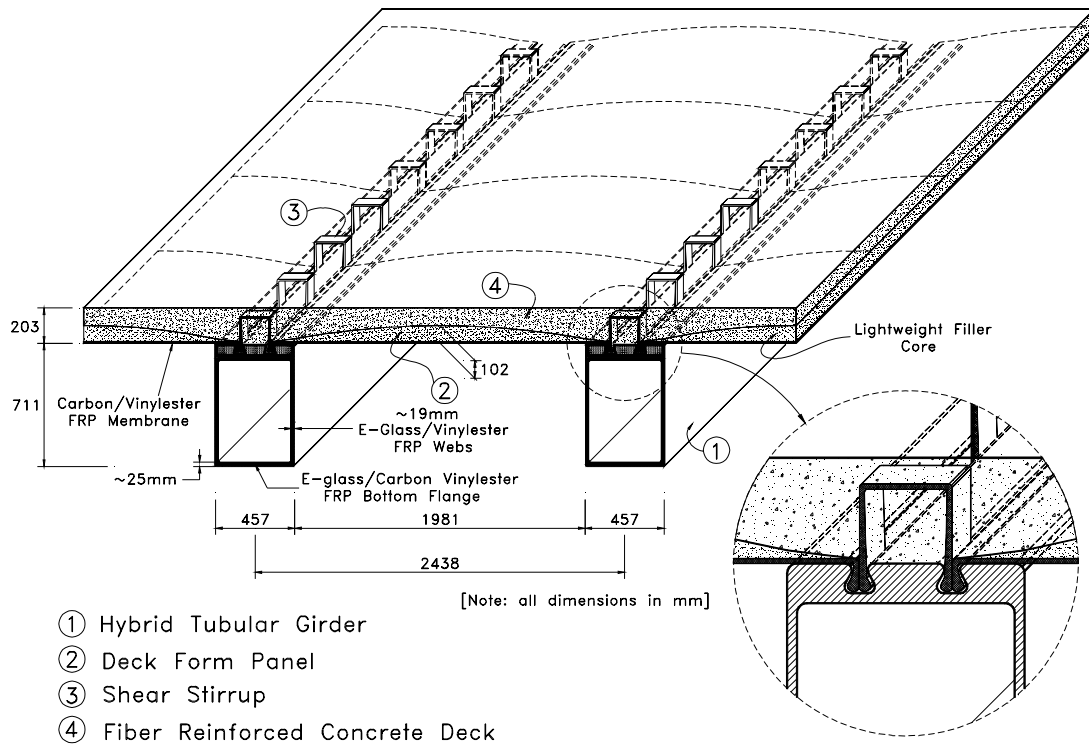
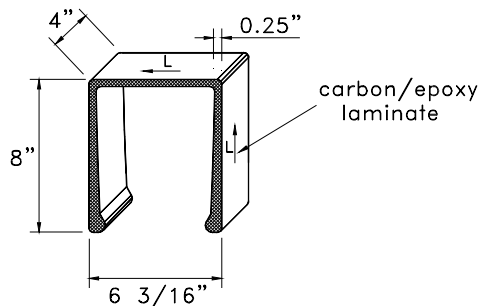


**Figure 1.4 Hybrid tube system**

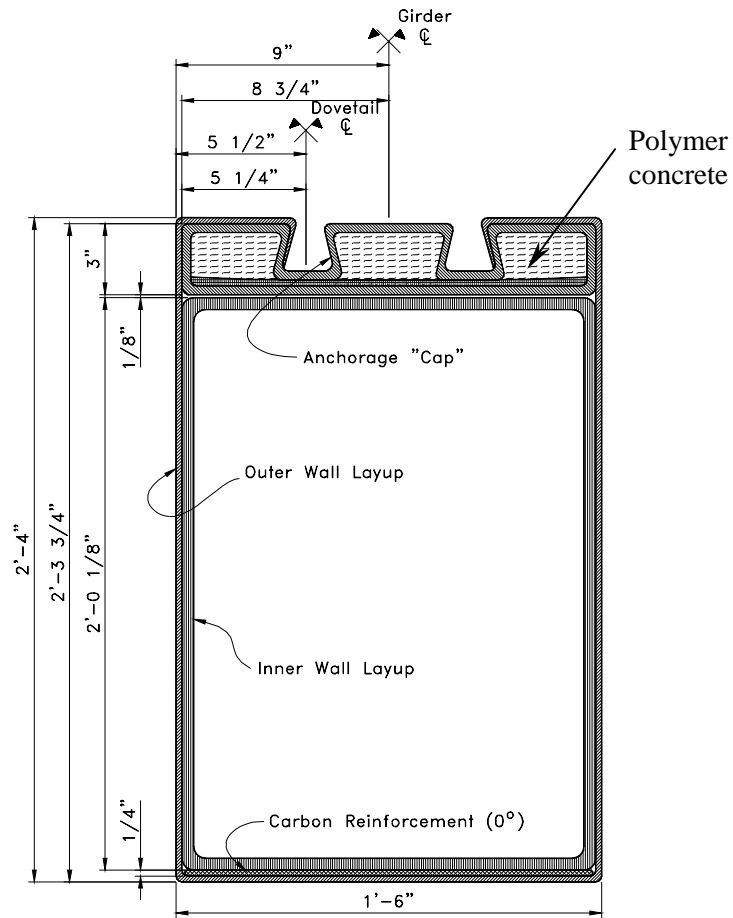


(1" = 25.4 mm)

**Figure 1.5 Geometry of carbon/epoxy shear connectors**

The hybrid girder consists of an E-glass-carbon/vinylester box beam with cross-sectional geometry as shown in Figure 1.6. The beam has an overall depth of 711 mm (28 in.), a width of 457 mm (18 in.), and a nominal web thickness of 19 mm (0.75 in.).

The geometry of the top flange is such that it provides an anchorage zone for the tension tie panels and the snap-in shear connectors. The overall height of the anchorage region is 98 mm (3.875 in.) with a E-glass/vinylester wall of 19 mm (0.75 in.) nominal thickness. The tube is hollow and the end-cap region is filled with polymer concrete. The bottom flange of the beam is reinforced with a 6-mm (0.25 in.)-thick uni-directional carbon fiber reinforced composite, which is embedded within E-glass/vinylester layers. The total nominal thickness of the bottom flange is 25 mm (1 in.).



(1'=305 mm, 1" = 25.4 mm)

**Figure 1.6 Hybrid girder cross-section**

The tension tie panel consists of a bottom plate, a foam core, and a thin top layer. The plate is prefabricated with a unidirectional carbon/epoxy composite that has E-glass/vinylester chopped strand mat (51 g/m<sup>2</sup> or 1 1/2 oz./yd<sup>2</sup>) face sheets on both surfaces. The parabolic-shaped polystyrene foam core is bonded to the plate. A thin E-glass fabric is then wet laid up on the top of the core.

The overall geometry of a tension tie panel unit is shown in Figure 1.7. The tension tie panels should be placed in segments along the transverse direction of the bridge.

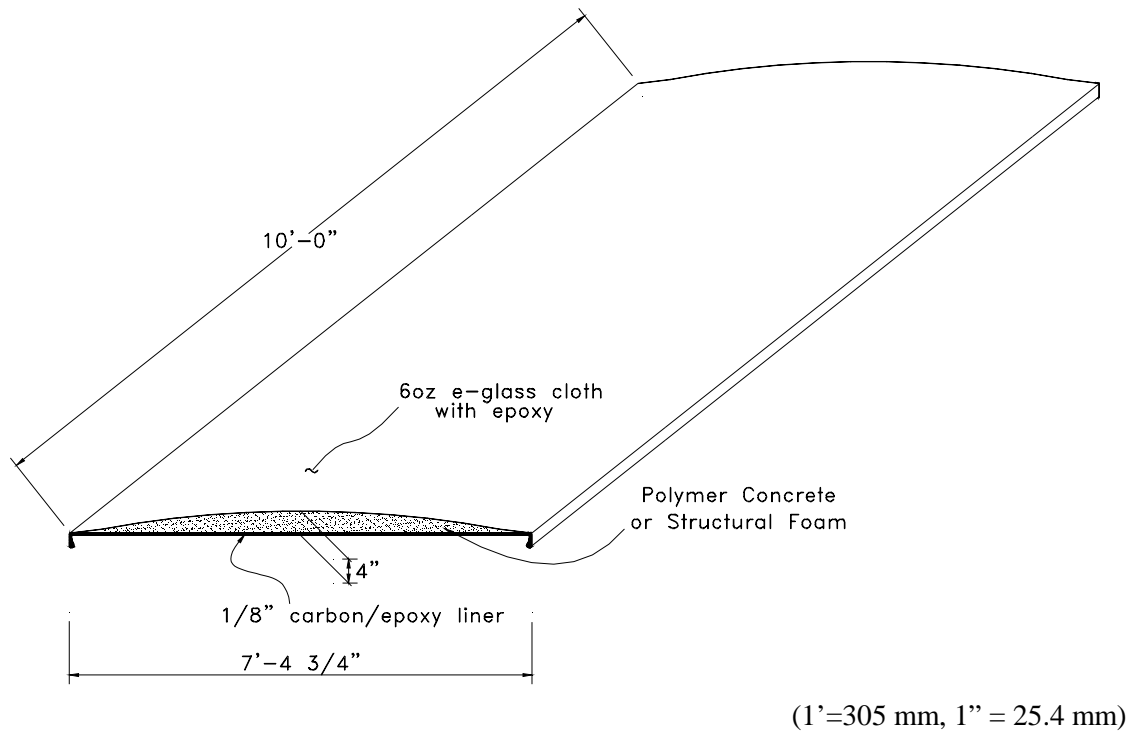


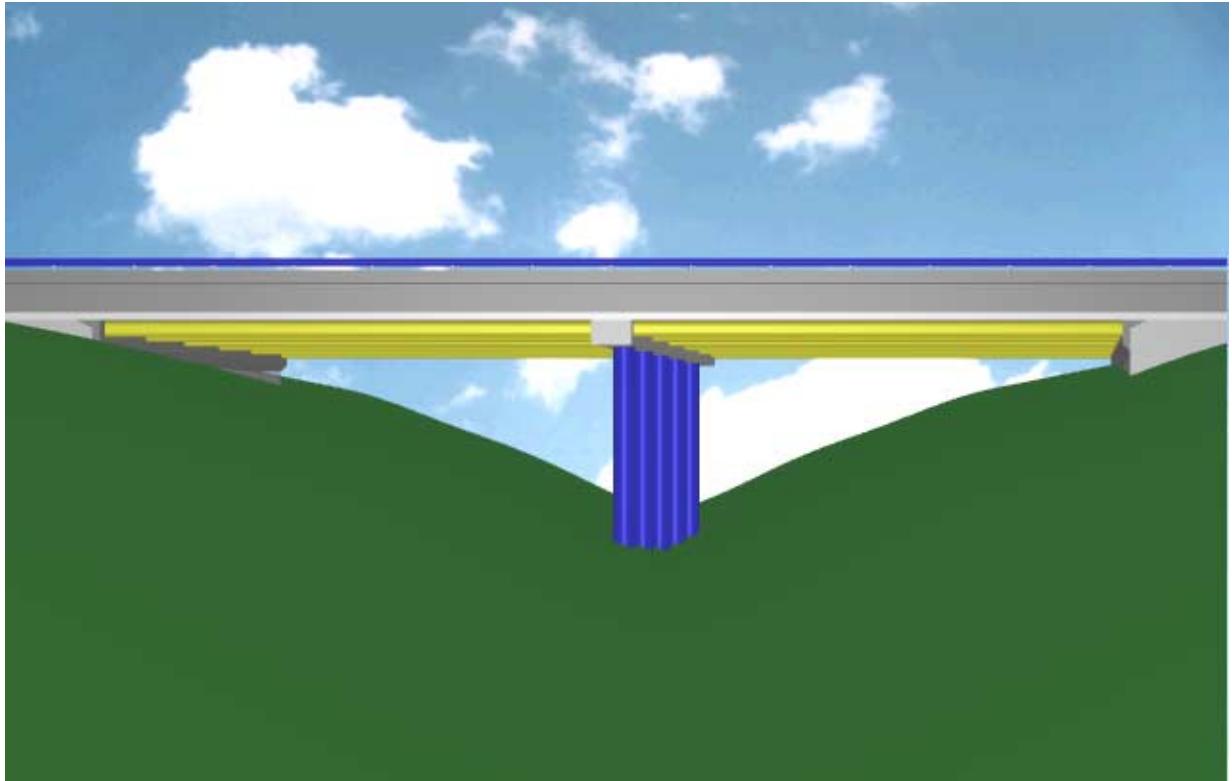
**Figure 1.7 Overall dimensions of the tension tie panel**

### 1.3 Applications

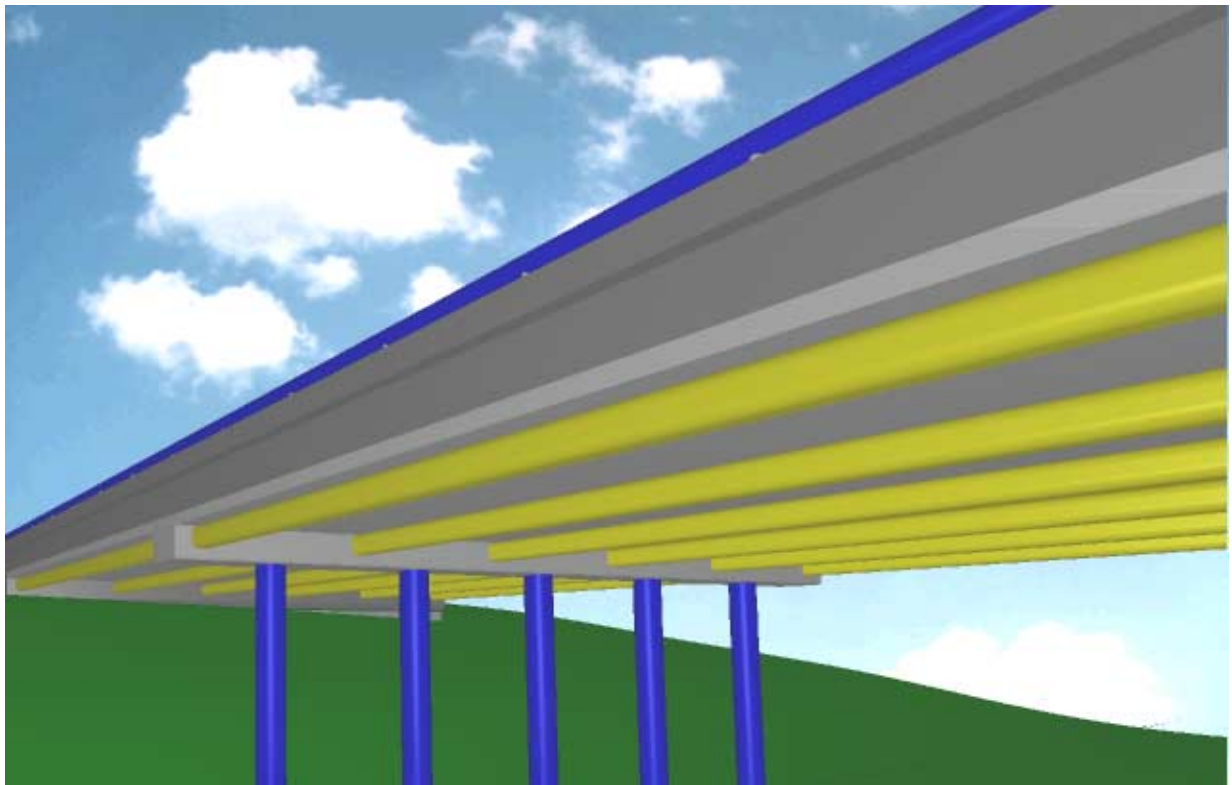
#### 1.3.1 Kings Stormwater Channel Bridge

The CSS concept is currently being considered by Caltrans in a demonstration bridge on California State Route 86 near the Salton Sea, the King Stormwater Channel Bridge. The carbon shell bridge design consists of a 20.1 m (66 ft) two-span continuous beam-and-slab type bridge with a five-column intermediate pier, see Figure 1.8 and Figure 1.9. Concrete filled carbon tubes comprise the longitudinal beams connected along their tops to a structural slab. The structural slab consists of an E-Glass Fiber Reinforced Polymer (GFRP) deck system.

The bridge cross-section selection was determined primarily by geometric constraints and structural performance requirements. The requirement for a shallow superstructure depth, approximately 762 mm (2.5 ft), constrained the geometric selection of the girders. The preliminary selection of the bridge components was based on structural performance and operational requirements, and was guided by previous experience in the design and full scale testing of advanced composite bridge components at the University of California, San Diego (UCSD).

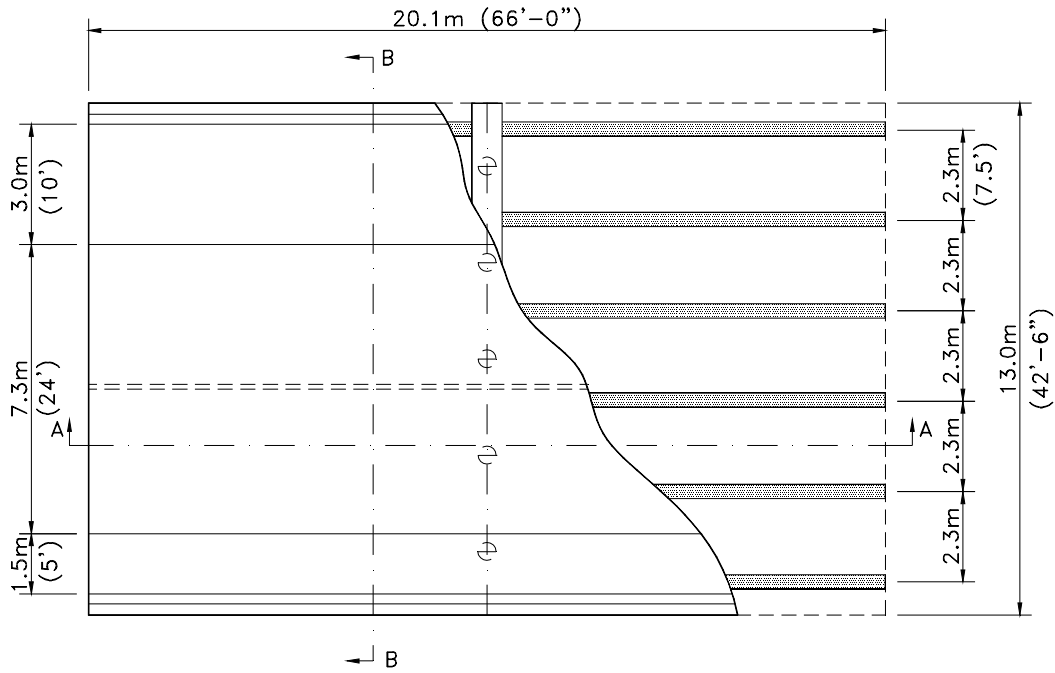


(a) Side View

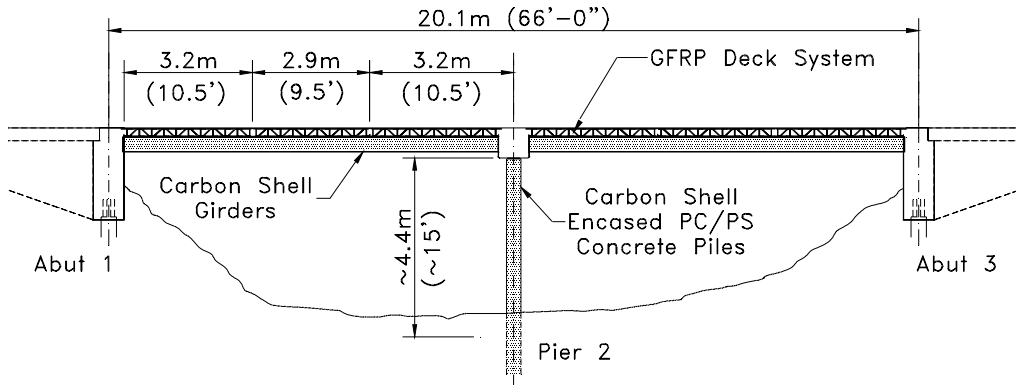


(b) Close-up view

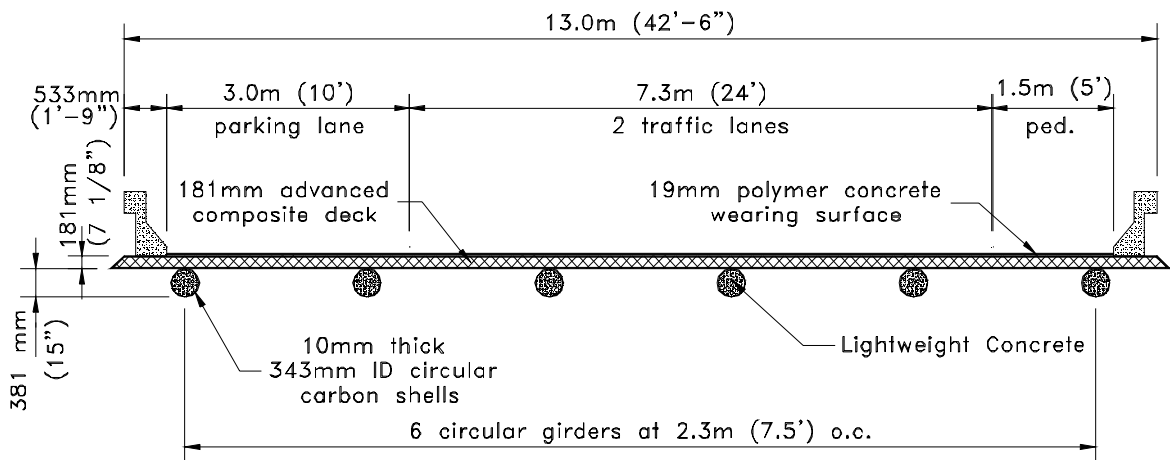
**Figure 1.8 Conceptual rendering of Kings Stormwater Channel Bridge**



a) Plan view



b) Longitudinal Section A-A



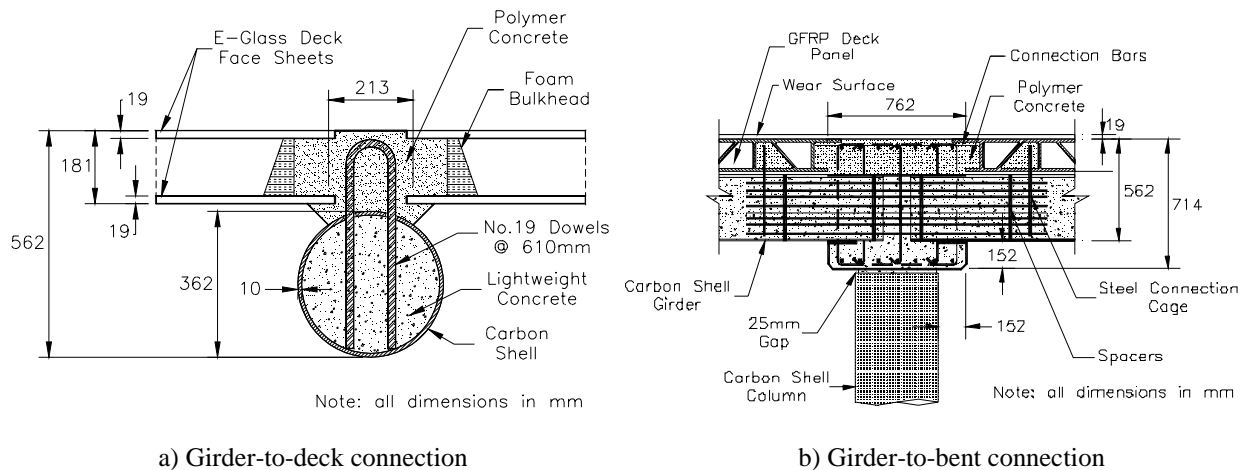
c) Transverse Section B-B

Figure 1.9 Kings Stormwater Channel Bridge geometry

The structural design features of the bridge are summarized in the following with reference to Figure 1.9

- Total bridge length of 20.1m (66 ft)
- Two 10 m (33 ft) span bridge system with a multi-column intermediate pier
- The bridge superstructure consists of a beam-and-slab deck type
- The cross section is 13 m (42-1/2 ft) wide, composed of 6 longitudinal girders spaced at every 2.3 m (7.5 ft).
- The overall superstructure height (excluding a 19 mm or 3/4” wear surface) is 562 mm (22-1/8 in.), with an average girder depth of 362 mm (14.25 in.) and an average slab depth of 181 mm (7.125 in.).
- The longitudinal girders consist of filament wound carbon/epoxy shells filled with lightweight concrete
- The slab consists of E-Glass Fiber Reinforced Polymer (GFRP) deck panels composed of pultruded trapezoidal sections with top and bottom skin layers.
- Conventional road barriers will be connected to the GFRP deck system.
- The multi-column intermediate pier is composed of precast prestressed concrete piles, with the two outer piles encased by circular carbon/epoxy shells to evaluate environmental degradation.
- The bridge structure uses conventional abutment details.

The longitudinal connections of the carbon shell girders and their connection to the E-glass deck system is achieved by means of conventional reinforcement. Details of the girder to deck and girder to bent connections are given in Figure 1.10.



**Figure 1.10 Kings Stormwater Bridge connection details**

### 1.3.2 I-5/Gilman advanced composite cable stayed bridge

The conceptual design of a 137 m (450 ft) long cable stayed two-lane traffic bridge across Interstate 5 at Gilman Drive (I-5/Gilman) on the University of California, San Diego (UCSD) campus, to be built with FRP composite materials, was developed as a preliminary design study in a cooperative agreement with the Federal Highway Administration (FHWA) [5]. The conceptual design was performed to demonstrate applications of both CSS and HTS concepts in civil infrastructure.

The I-5/Gilman Advanced Technology Bridge is a 137.2 m (450 ft.) long cable-stayed bridge supported by a 57.9 m (190 ft) high A-frame pylon, designed utilizing FRP composite materials and manufacturing. The bridge system is that of a dual plane, fan-type, cable-stayed bridge with an eccentric A-type pylon. The overall concept of the I-5/Gilman cable-stayed bridge is depicted in Figure 1.11, Figure 1.12 and Figure 1.13. The superstructure has an overall width of 18.3 m (60 ft) and a structural depth of ~1.45 m (4.75 ft). The bridge structure is designed to accommodate two 3.7 m (12 ft) lanes of AASHTO HS-20 loading, two bicycle lanes, two 1.52 m (5 ft) pedestrian walkways, and two utility service tunnels.

The design concept consists of the dual cable plane system supporting concrete filled carbon/epoxy tubes, connected in the transverse direction by hybrid E-glass-carbon reinforced FRP hollow cross-beams spaced 2.4 m (8 ft) on center, which in turn support a longitudinally spanning fiber-reinforced concrete deck. The system considers a set of cables at every 4.9 m (16 ft). A fixed support condition at the west abutment, for torsional rigidity, and a roller support condition with torsional restraint at the east abutment allows thermal expansion movements. The single A-frame type pylon system is located on the west side of the freeway, allowing a dual set of stays radiating outward towards the edge beams. The design uses conventional concrete abutments and foundations. The primary structural components in I-5/Gilman Advanced Composite Cable Stayed Bridge are the deck system, the longitudinal edge girders, the transverse beams, the pylon, and the cable stays.

The superstructure, schematically shown in Figure 1.14, consists of two longitudinal carbon/epoxy/concrete edge girders, 13.7 m (45 ft) apart, connected in the transverse direction by hybrid E-glass-carbon reinforced transverse girders, which in turn support a polypropylene fiber reinforced concrete arching deck.

The longitudinal edge girders are based on the concrete filled Carbon Shell System construction concept described in Section 1.1. The concrete filled Carbon Shell System allows for new structural elements consisting of prefabricated filament-wound carbon/epoxy thin shells filled on-site with concrete. Transverse ribs are provided on the inside of the carbon/epoxy shell for full force transfer between the concrete in-fill and the shell. The concept is suitable for both columns and girders. The girder carbon/epoxy shell members consist of circular tubes of 91 cm (3 ft) inner diameter and a wall thickness of 10 mm (0.375 in.). The carbon/epoxy tubes are fully grouted with normal weight concrete to (1) stabilize the carbon/epoxy shell, (2) aid the member to carry the stay compressive forces, and (3) provide anchorage of the cable anchorage hardware. Structurally, composite action between the concrete filled tubes and the deck is achieved through the use of shear dowels. The longitudinal girders are prestressed, prior to the installation of the transverse system, in the part of the span close to the east abutment.

The Hybrid Tube System (HTS) described in Section 1.2 constitutes the transverse deck system for the superstructure. The system uses hollow hybrid E-glass-carbon reinforced FRP beams connected along their tops with a polypropylene fiber reinforced concrete arching deck as shown in Figure 1.4. The girders are E-glass/vinylester rectangular box sections with longitudinal carbon reinforcement in the bottom flange. The hollow E-glass-carbon reinforced FRP box beams straddle the longitudinal carbon/epoxy shells spaced at every 2.4 m (8 ft) on center along the bridge length.



**Figure 1.11 Rendering of the I-5/Gilman Advanced Technology Bridge**

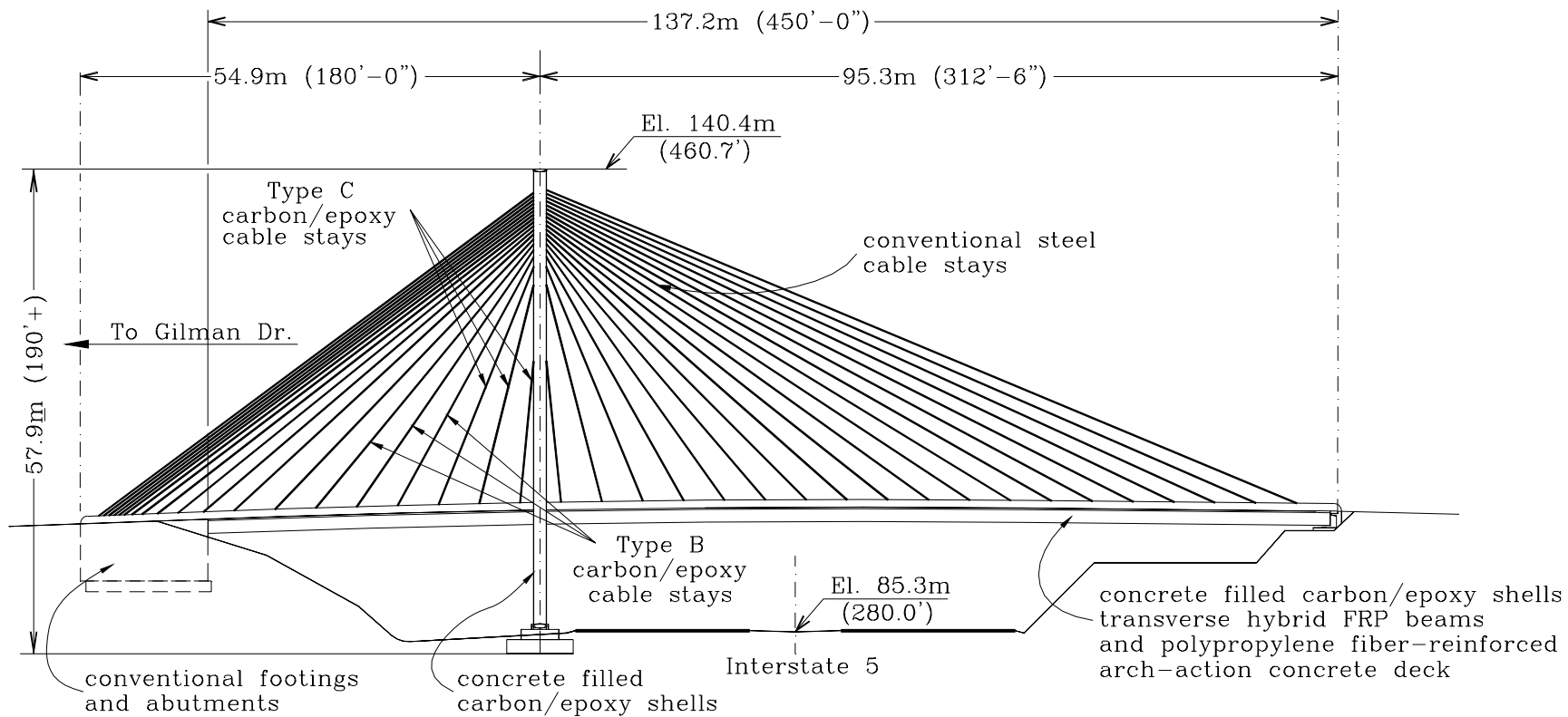


**Figure 1.12 Elevation of the I-5/Gilman Advanced Technology Bridge--geometry and components**

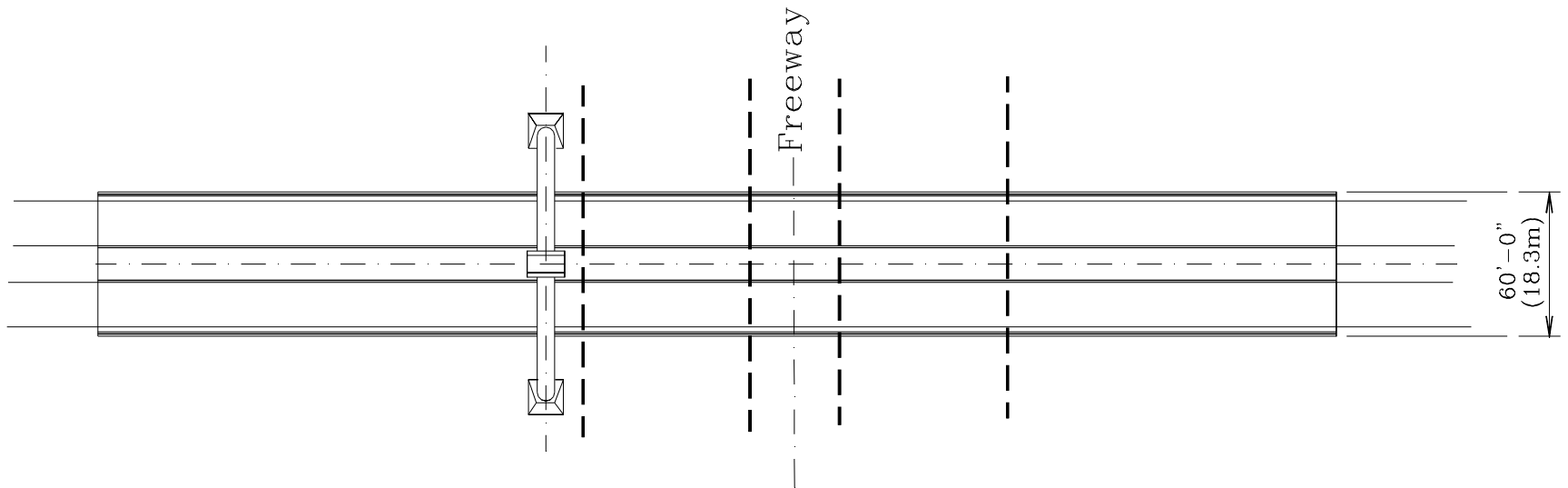
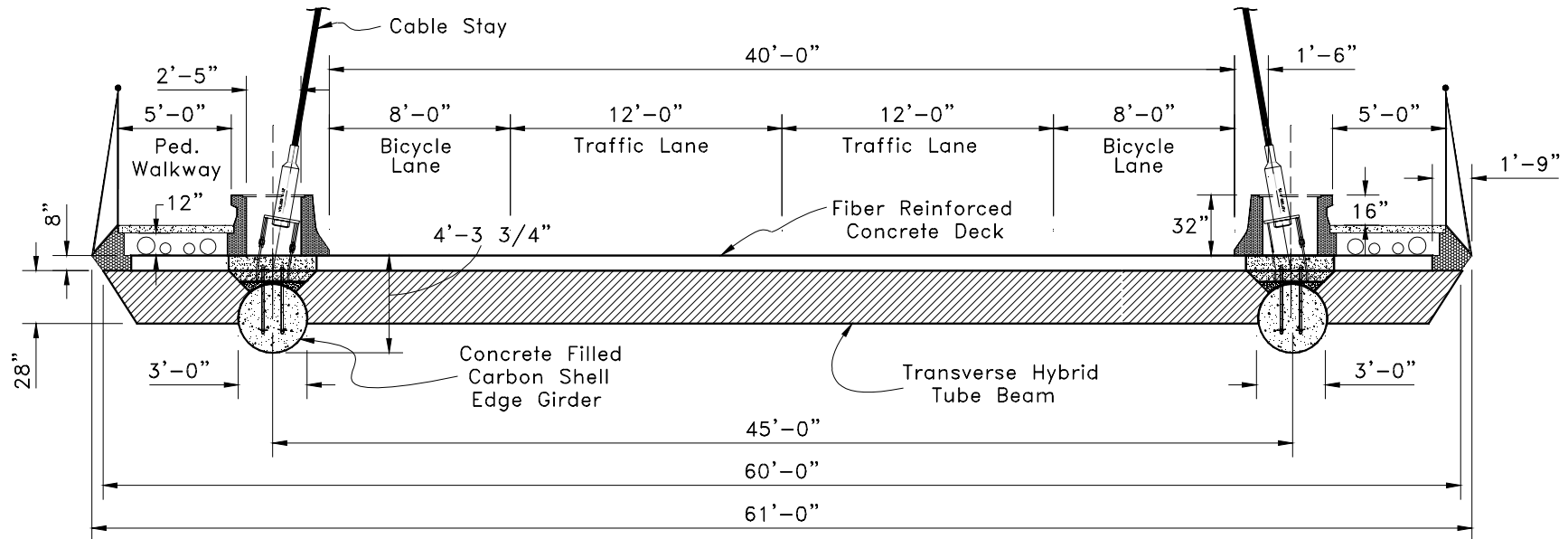


**Figure 1.13 Plan view of the of I-5/Gilman Advanced Technology Bridge**



(1'=305 mm, 1"=25.4 mm)

**Figure 1.14 I-5/Gilman Bridge superstructure section**

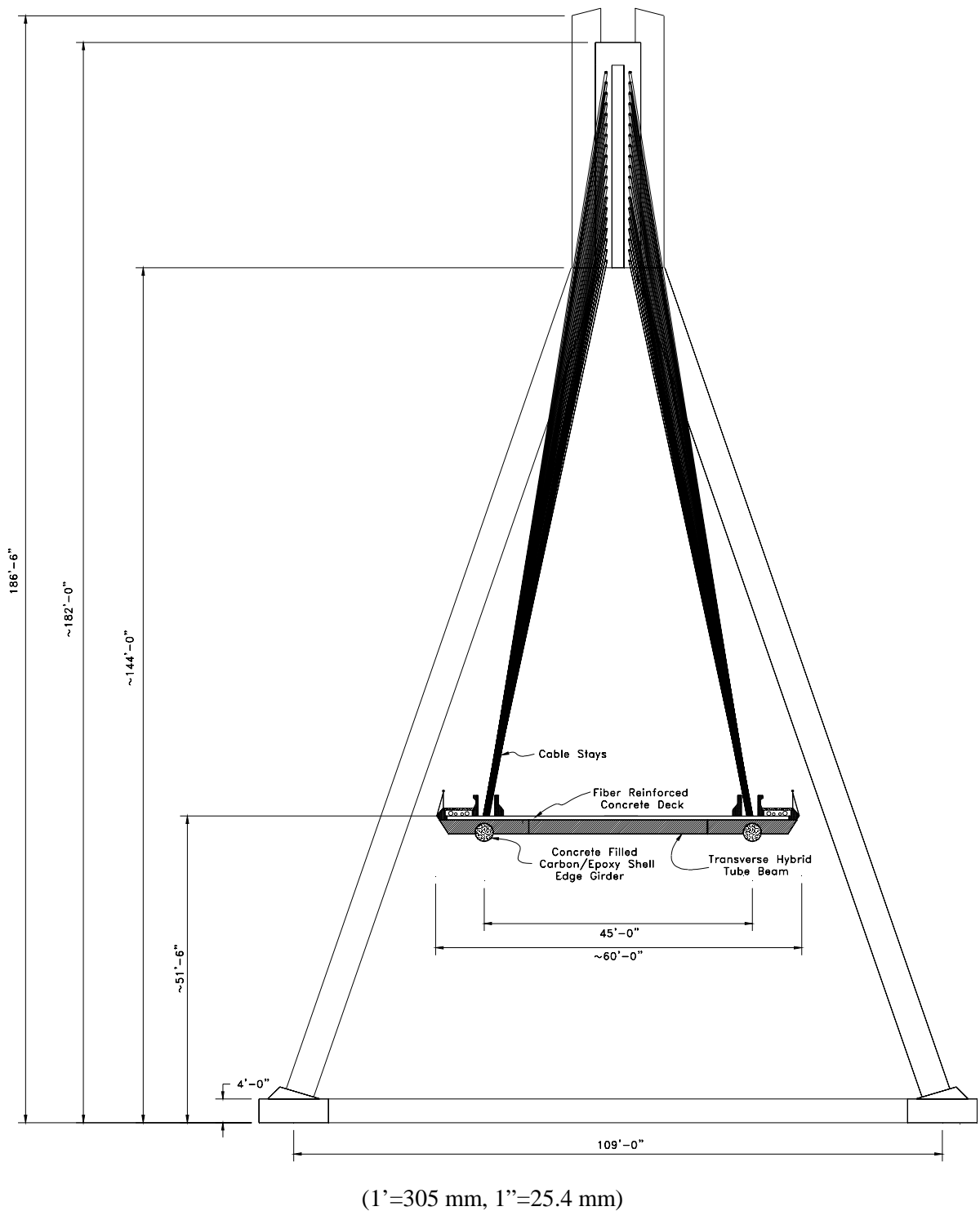


**Figure 1.15 Cross-section view of I-5/Gilman Advanced Technology Bridge**

An FRP form panel (see Figure 1.7) is snap-locked to the pultruded girders providing a tension tie between girders and the stay-in-place form for a fiber reinforced arch-action-type concrete deck. Normal

weight concrete is used for the slab. Prefabricated carbon/epoxy snap-in stirrups (see Figure 1.5) provide the horizontal shear transfer between the concrete deck and the hybrid tubes.

The delta shaped pylon concept is shown in Figure 1.15. Pylon dimensions of approximately 57.9 m (190') in height and 1.52 m (5 ft) in diameter, were selected based on aesthetic, economic, and engineering considerations. The concrete filled carbon shell system is also used for the pylon system. The pylon carbon/epoxy shell members consist of circular tubes of 1.52 m (5 ft) inside diameter and a wall thickness of 13 mm (0.50 in.). The carbon/epoxy tubes are fully grouted with normal weight concrete to (1) stabilize the carbon/epoxy shell and (2) aid the member to carry the stay compressive forces.

Due to cost considerations, conventional steel cable-stays are mainly used for the I-5/Gilman Bridge. Only six to eight of the cable stays will be made from FRPs with FRP composite anchorage technology.

## 1.4 Scope of The Report

The scope of this report is a preliminary evaluation of the Modular Hybrid Tube System. To investigate the structural behavior of the HTS system, a series of tests were conducted at the Charles Lee Powell Structures Laboratory, at UCSD. Initially the material properties of all the HTS components utilized are obtained as explained in Chapter 2. Chapter 3 describes the flexural characterization of the hybrid girder, which was performed by means of a four-point-bending test. An HTS subassemblage consisting of a two girder-concrete deck was then tested under flexure and punching-shear as reported in Chapter 4. Conclusions of this preliminary evaluation are given in Chapter 5.

## 2 MANUFACTURING AND MATERIAL PROPERTIES OF THE COMPONENTS

### 2.1 Materials Specifications

#### 2.1.1 FRP composites

Three types of fabrics are used in the lay-up of the composite girder. They are summarized in Table 2.1. The nominal properties of these fibers are shown in Table 2.2.

**Table 2.1 Summary of fabrics used in the composite girder**

Fabric Designation	Fiber type	Areal Weight g/m <sup>2</sup> (oz/yd <sup>2</sup> )	Fiber Orientation	Basis Weight (%)
CDB340	E-glass	1153 (34)	0°/45°/-45°	50/25/25
A260	E-glass	881 (26)	0°	100
GA130	Carbon	441 (13)	0°	100

**Table 2.2 Nominal fiber properties**

Fiber	Young' Modulus, GPa (msi)	Tensile Strength, MPa (ksi)
E-glass	72.4 (10.5)	1862 (270)
Carbon	228 (33)	3932 (570)

Vinylester resin is used in the FRP composite components. The nominal properties of the resin are summarized in Table 2.3.

**Table 2.3 Resin properties**

Resin type	Vinylester	Epoxy
Elastic Modulus, GPa (msi)	3.45 (0.50)	4.27 (0.62)
Tensile strength, MPa (ksi)	75.9 (11.0)	77.9 (11.3)
Compressive strength, MPa (ksi)	372 (54.0)	120 (17.4)

### 2.1.2 Fiber-reinforced concrete

Polypropylene fibers are used in the fiber-reinforced concrete deck. The physical properties of the fibers are summarized in Table 2.4.

**Table 2.4 Physical properties\* of polypropylene fibers**

Material	Virgin homopolymer polypropylene
Form	Collated fibrillated twisted-bundle fiber
Specific Gravity	0.91
Tensile Strength, MPa (ksi)	621-759 (90-110)
Lengths, mm (in)	60 (2.36)
Color	Tan
Acid/Alkali resistance	Excellent
Absorption	Nil
Compliance	ASTM C-1116

\* Provided by Forta®

## 2.2 Manufacturing of FRP Components

In order to assess the structural response at a prototype level, the FRP components were fabricated using the wet lay-up process with E-glass and carbon fabrics rather than through pultrusion. This is done to enable the use of cheaper tooling such as wooden or foam molds during the initial investigation, thereby avoiding the initial capital cost of metal dies for pultrusion. Due to the large thickness of these components (2.5 cm or 1" to 3.8 cm or 1.5"), lay-up was done in steps to avoid excessive exothermic problems. Between each two steps, the surfaces were allowed to ambient temperature level, then ground, and primed with fresh resin. Plastic rollers were used to apply the fabric layers (as shown in Figure 2.1).



**Figure 2.1 Resin being applied to the girder with plastic rollers**

A schematic showing the steps in making the hybrid girders is given in Figure 2.2. A mandrel was first built by bonding tooling foam onto wood blocks. Glass fabric was then placed on the surface of the mandrel by wet lay-up. This forms the inner tube of the hybrid girder. After the resin cures, the mandrel is pulled out of the tube by breaking the tooling foam. A cap, which is also made with wet lay-up on a separate mandrel, is then bonded on the top of the tube. Unidirectional carbon fabric was then laid up on the bottom of the tube. Finally, an outer skin was wrapped around the girder.

Lay-up details are given in Figure 2.3.

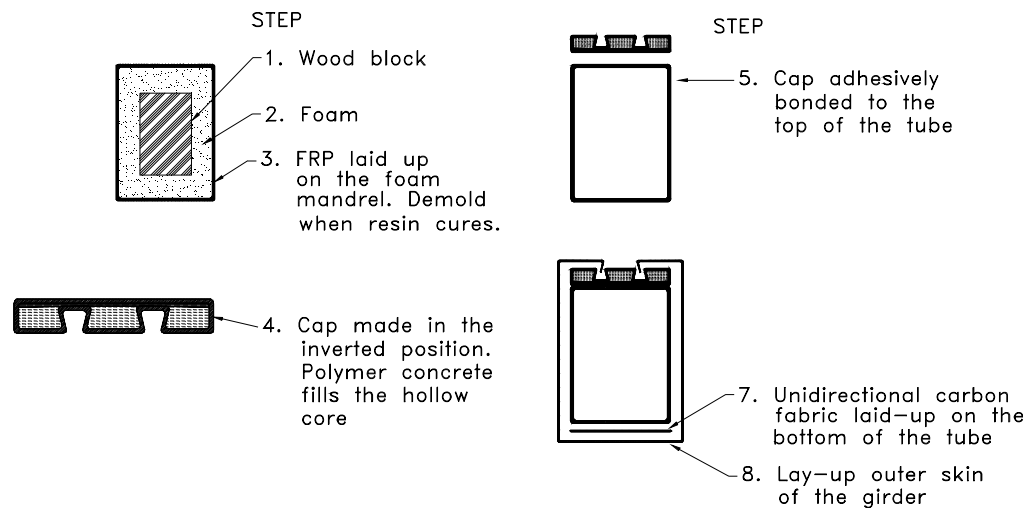
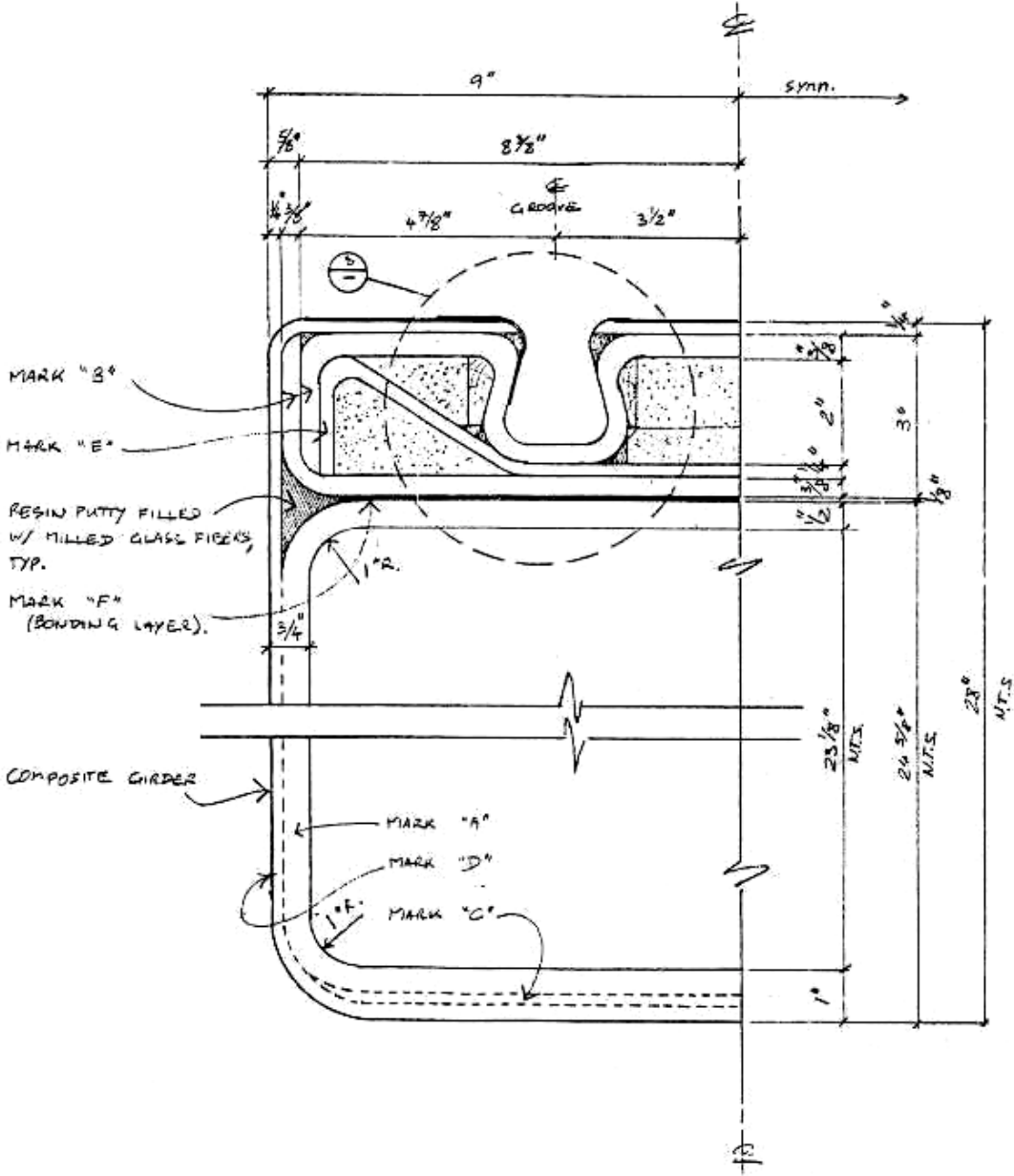


**Figure 2.2 Manufacturing schematic of the hybrid girder**

For the convenience of manufacturing, the details in the cap of the girder were modified from its original design as shown in Figure 1.6 and are shown in the shop drawing (Figure 2.3). The “Mark” definitions related to the fabric lay-up in the drawing are given in Table 2.5.



(1"=25.4 mm)

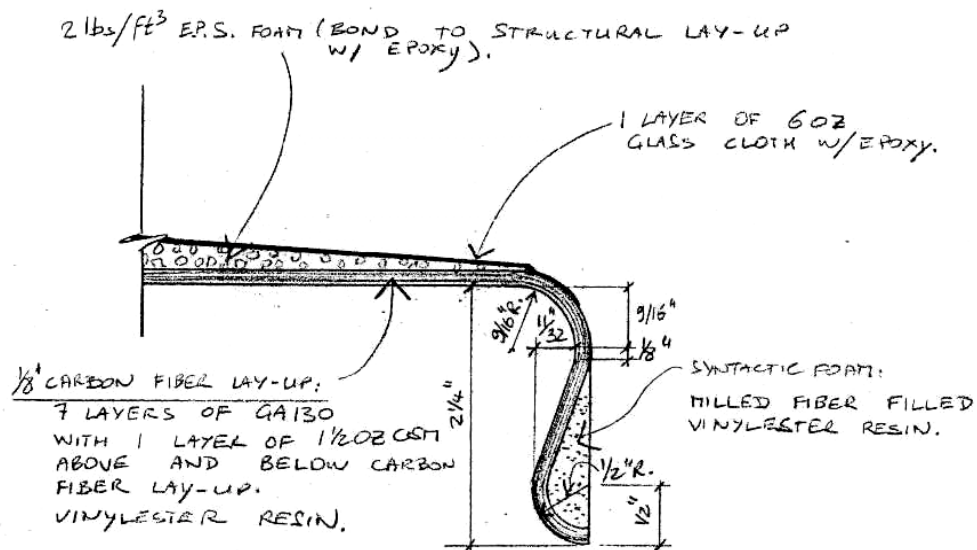
Figure 2.3 Shop drawing for the FRP girder (showing lay-up details)

**Table 2.5 Mark definitions for the lay-up of the hybrid girders (as in Figure 2.3)**

Lay-up Name	Successive Plys	Number of Plys	Ply Name	Fabric	Orientation
Mark "A"	A'	1	A	CDB340	0°/-45°/45°
	A	3	A'	CDB340	90°/45°/-45°
	A'	1	B	A 260	0°
	B	1	B'	A 260	90°
	A	1	C	GA 130	0°
	A'	2	D	1.5 OZ CSM*	N/A
Mark "B"	B'	1			
	A	5			
	B'	1			
Mark "C"	C	13			
	A'	2			
Mark "D"	A	1			
	B	1			
Mark "E"	B'	1			
	B	3			
	B'	1			
Mark "F"	D	1			
	B	1			
	D	1			

\* Glass fiber chopped strand mat.  
Areal weight 51 g/m<sup>2</sup> (1.5 oz/yd<sup>2</sup>)

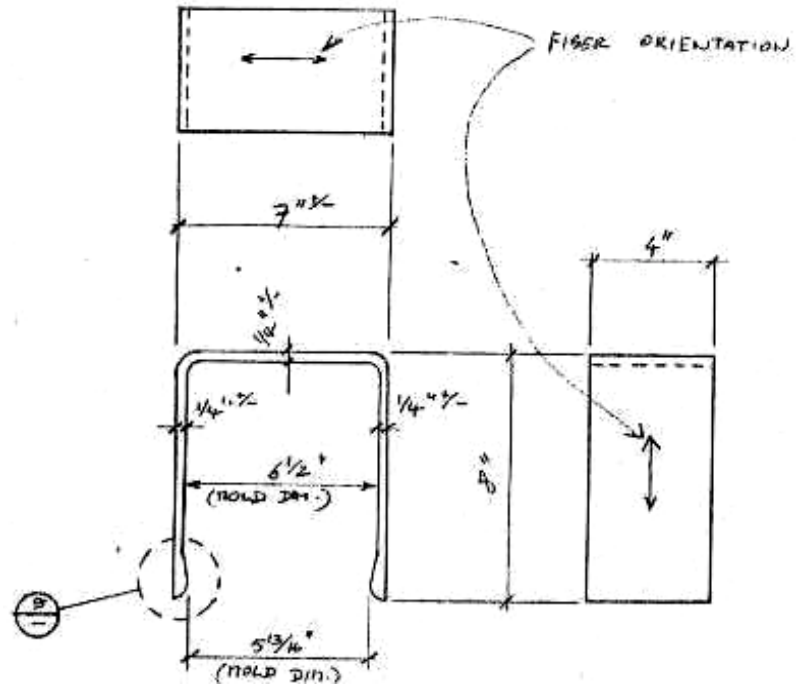
The bottom of the tension panels is first laid up with unidirectional carbon fabric on a flat surface. The edges of the panel have the contour as shown in the shop drawing (Figure 2.4). A pre-shaped foam core is then bonded to the top of the tension panel. Finally, a thin (6 oz./yd<sup>2</sup> or 203 g/m<sup>2</sup>) glass fabric is laid on the top of the foam core.



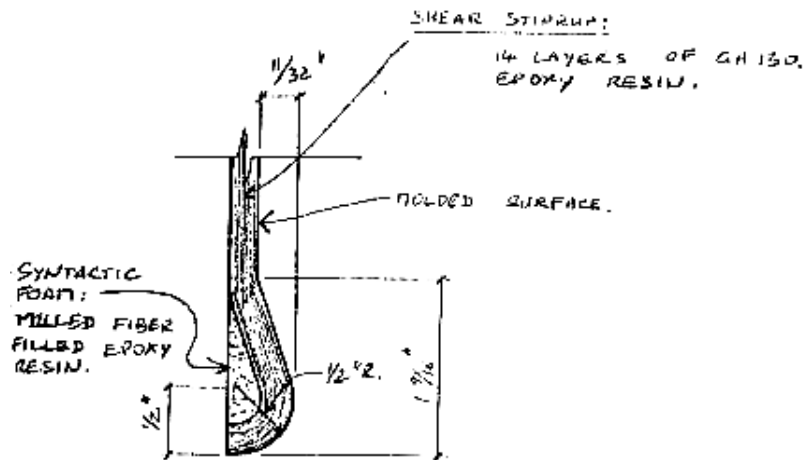
(1"=25.4 mm)

**Figure 2.4 Shop drawing for the edge detail of the tension panel**

The shear stirrups are made with a male mold, which accommodates the details as shown in Figure 2.5.



(a) Stirrup dimension



(b) Leg detail

(1"=25.4 mm)

Figure 2.5 Shop drawing for the edge detail of the shear stirrup

### 2.3 FRP Hybrid Girder

The majority of the girder cross-section is composed of an E-glass/vinylester laminated composite. The fiber volume fraction is approximately 33%. The design of the glass laminate was guided by the

objective of achieving a wall thickness of approximately 19 mm (0.75”) to provide restraint against buckling. The lamina definition is given in Table 2.6. The resulting mechanical properties of the girder are summarized in Table 2.7. The hybrid girder weighs approximately 149 kg per linear meter (100 lb per liner foot).

**Table 2.6 Lamina Information and Nomenclature**

Ply Name	Fabric Nomenclature	Placement of fabric	Nominal Layer Thickness, mm (in)
A	CDB340	0°	1.4 (0.055)
A'	CDB340	90°	1.4 (0.055)
B	A260	0°	1.2 (0.046)
B'	A260	90°	1.2 (0.046)
C	GA130	0°	0.45 (0.018)

**Table 2.7 Mechanical Properties of Hybrid Girder**

Property	Webs (Girder)	Webs (Cap)	Top Flange (Cap)	Bot. Flange (Cap)	Bot. Flange (Girder)
Longitudinal Modulus, $E_L$	14000 MPa (2.03e6 psi)	15255 MPa (2.21e6psi)	14621 MPa (2.12e6 psi)	15862 MPa (2.30e6 psi)	42069 MPa (6.10e6 psi)
Transverse Modulus, $E_T$	12552 MPa (1.82e6 psi)	12793 MPa (1.86e6psi)	12552 MPa (1.82e6 psi)	12138 MPa (1.76e6 psi)	12276 MPa (1.78e6 psi)
In-Plane Shear Modulus, $G_{LH}$	4428 MPa (6.42e5 psi)	3647 MPa (5.29e5 psi)	4145 MPa (6.01e5 psi)	3538 MPa (5.13e5 psi)	4448 MPa (6.45e5 psi)
In-Plane Poisson's Ratio, $\nu_{LH}$	0.33	0.29	0.31	0.30	0.31
In-Plane Poisson's Ratio, $\nu_{HL}$	0.30	0.24	0.27	0.23	0.13
Density, $\gamma$	17.7 kN/m <sup>3</sup> (0.065 lb/in <sup>3</sup> )	17.1 kN/m <sup>3</sup> (0.063 lb/in <sup>3</sup> )			
Long. Coef. of Thermal Expansion	7.36e-5 /°C (4.09e-5 /°F)	7.11e-5 /°C (3.95e5 /°F)	7.16e-5 /°C (3.98e-5 /°F)	6.53e-5 /°C (3.63e-5 /°F)	2.56e-5 /°C (1.42e-5 /°F)
Transv. Coef. of Thermal Expansion	9.13e-5 /°C (5.07e-5 /°F)	9.81e-5 /°C (5.45e-5 /°F)	9.59e-5 /°C (5.33e-5 /°F)	10.62e-5 /°C (5.90e-5 /°F)	9.00e-5 /°C (5.00e-5 /°F)
Nominal Thickness	19 mm (0.75 in.)	25 mm (1.0 in.)	15 mm (0.6 in.)	30 mm (1.2 in)	25 mm (1.0 in.)

## 2.4 Shear Stirrups

The shear connectors consist of prefabricated carbon/epoxy unidirectional composite. The shear connectors have a thickness of 6.4 mm (0.25 in.). The lay-up calls for 14 plies of GA130 as in the following sequence: The nominal properties of the stirrups are shown in Table 2.8.

**Table 2.8 Nominal properties of carbon/epoxy composite in the shear stirrup and the tension panel**

Property	SI Units	English Units
Longitudinal* Modulus, $E_L$	103 GPa	15.0e6 psi
Transverse (Hoop) Modulus, $E_T$	8.5 GPa	1.23e6 psi
In-Plane Shear Modulus, $G_{LH}$	3.6 GPa	5.25e5 psi
In-Plane Poisson's Ratio, $\nu_{LH}$	0.28	0.28
Density, $\gamma$	15.7 kN/m <sup>3</sup>	5.78e-2 lb/in <sup>3</sup>
Long. Coef. of Thermal Expansion	5.87e-7 mm/mm/°C	3.26e-7 in/in/°F
Transv. Coef. of Thermal Expansion	3.01e-5 mm/mm/°C	1.67e-5 in/in/°F

\* The longitudinal direction of the stirrup is circumferential to the hybrid girder direction.

## 2.5 Tension Tie Panels

The unidirectional carbon composite in the bottom plate of the tension tie panel has the same properties as those shown in Table 2.8. The longitudinal direction of the tension panel is perpendicular to that of the hybrid girder.

Each 2.44 m x 3.05 m (8'x10') tension panel weighs approximately 445 N (100 lbs) and can be carried by two people.

## 2.6 Concrete

A volume fraction of 0.6% (equivalent to 5.45 kg/m<sup>3</sup> or 9.2 lb/yd<sup>3</sup> of concrete) of polypropylene fibers was used in the fiber reinforced concrete mix. The purpose of the fibers is to control shrinkage cracks in the unreinforced concrete slab.

A series of tests were conducted to compare properties of concrete of different mix designs—lightweight versus normal weight, fiber-reinforced versus plain. The results of these tests are summarized in this Section.

All concrete cylinders and the slab of the system have a nominal strength of 34.5 MPa (5 ksi) and design slump of 10 cm (4 inches). The concrete weighs approximately 150 lb/ft<sup>3</sup> (2400 kg/m<sup>3</sup>) for normal-weight and 2083 kg/m<sup>3</sup> (130 lb/ft<sup>3</sup>) for lightweight. When the polypropylene fibers are added to the concrete mix, the slump of the mix decreases dramatically. Extra water was added to regain the needed 10 cm (4 inches) of slump. When casting the slab of the 2-girder subassembly, 113.6 liters (30 gallons) of extra water was added to the mix for this purpose. The effective water-to-(cement+flyash) ratio was increased from 0.41 to 0.44.

**Table 2.9 A summary of concrete mixes**

ID	1	2	3	4
Concrete type	LW		NW	
	Plain	FR	Plain	FR
Application	TC	TC	TC 2G	TC 2G
Design 28-day strength, MPa (ksi)	34.5 (5)	34.5 (5)	34.5 (5)	34.5 (5)
Design slump, cm (in)	10 (4)	10 (4)	10 (4)	10 (4)
Design W/C	0.43	0.41*	0.41	0.41*

\* Water-to-(cement+flyash) ratio. Extra water added to achieve the needed slump.

NW: Normal weight  
LW: Lightweight

TC: Test cylinders  
2G: Two-girder subassemblage  
FR: Fiber reinforced

### 2.6.1 Compressive properties

The compressive strength of the concrete was obtained from cylinder tests following ASTM C39-93a. The specimens were tested at 3-, 7-, 14-, 21- and 28-day periods. The curves of strength development over time are shown in Figure 2.6. The fibers have little effect on the compressive strength of the cylinders. The difference occurs after the failure: the unreinforced concrete specimen breaks into pieces while the fiber reinforced cylinder is held together by the fibers.

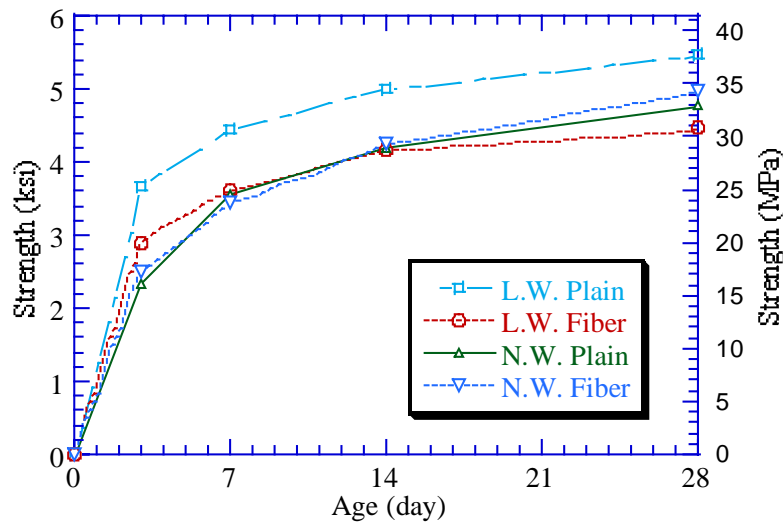


**Figure 2.6 Compressive strength development of the concrete cylinders**

### 2.6.2 Split-tension properties

The split tension strength of the concrete was obtained from cylinder tests following ASTM C496-90. The specimens were tested at 3-, 7-, 14-, 21- and 28-day periods. The curves of strength development over time are shown in Figure 2.7. The fibers have little effect on the split tension strength of the cylinders. The difference occurs after the failure: the unreinforced concrete specimen breaks into

two halves, whereas the two halves from the fiber reinforced cylinder are held together by the fibers bridging the crack..

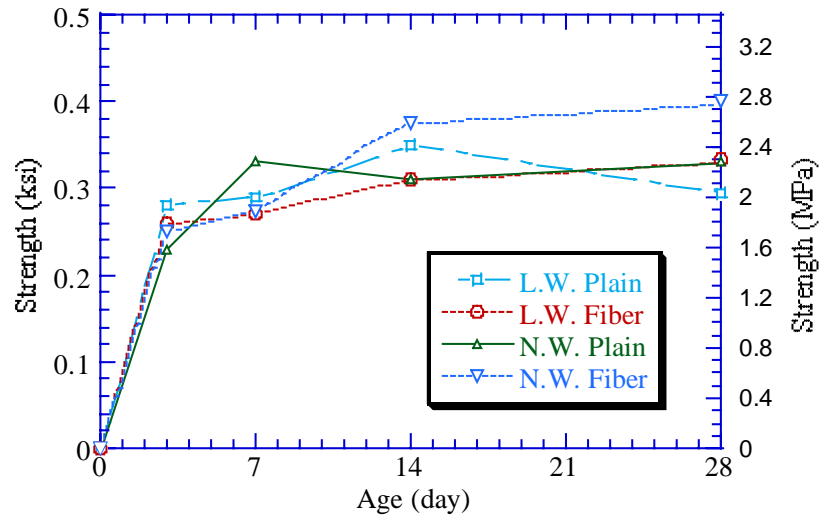


Figure 2.7 Split tension strength development of the concrete cylinders

### 2.6.3 Modulus of rupture

The rupture modulus was obtained from beam tests per ASTM C293-94. The results are summarized in Table 2.10. A slight increase in rupture modulus was seen in fiber-reinforced specimens.

### 2.6.4 Summary of concrete properties

The 28-day strength of the concrete specimens discussed in Sections 2.6.1 to Section 2.6.3 is summarized in Table 2.10

Table 2.10 Summary of 28-day properties of concrete specimens

Concrete type	Compressive strength MPa (ksi)	Split-tension strength MPa (ksi)	Modulus of rupture MPa (ksi)
Normal weight without	32.9 (4.77)	2.34 (0.340)	5.48 (0.795)
Normal weight fiber-reinforced	34.2 (4.96)	2.96 (0.430)	5.90 (0.855)
Lightweight without fiber	37.8 (5.48)	2.02 (0.293)	3.48 (0.504)
Lightweight Fiber-reinforced	30.8 (4.47)	2.30 (0.334)	3.98 (0.577)

The mix designs for normal weight concrete, fiber-reinforced and plain, were used in constructing the hybrid system test. One third of the slab (in system length direction) is cast with plain concrete and the other two thirds is cast with fiber reinforced concrete (shown in Figure 4.27). During the construction of the two-girder subassembly, the mix appeared too dry to be boom-pumped. Extra

water of approximately 16.5 liter/m<sup>3</sup> (3.33 gal/yd<sup>3</sup>) was added to the mix to obtain a needed workability. The measured slump was 11.4 cm (4.5 in.). Results from cylinders tests conducted at the day of the test were summarized in Table 2.11.

**Table 2.11 Properties of the concrete slab**

Concrete type	Compressive strength	Split-tension strength
	MPa (ksi)	MPa (ksi)
Plain	31.6 (4.58)	2.74 (0.398)
Fiber-reinforced	27.3 (3.96)	2.35 (0.342)

### 3 FLEXURAL TEST OF A HYBRID TUBE GIRDER

#### 3.1 Test Setup

The test was conducted in three steps. Step 1 is the initial stiffness characterization. It uses two servo-controlled hydraulic actuators to apply pseudo-static loading. The testing configuration is shown in Figure 3.1. Steps 2 and 3 both use two loading beams, each loaded by two hydraulic jacks (see Figure 3.2). Step 2 consists of loading up to the equivalent service load level (667.5 kN or 150 kip of total load) and holding the configuration at that level for 24 hours to assess potential strength or stiffness degradation. Step 3 is to increase the load up to failure.

The jacks have a stroke of 15 cm (6 inches), less than needed to fail the beam. They were first loaded to their full stroke before the stroke was reset with the help of two additional tie-down beams. Figure 3.3 shows that there are four beams on top of the girder. The two exterior ones are the loading beams and the interior ones are the tie-downs. Symmetric pseudo-static loading was applied up to failure.

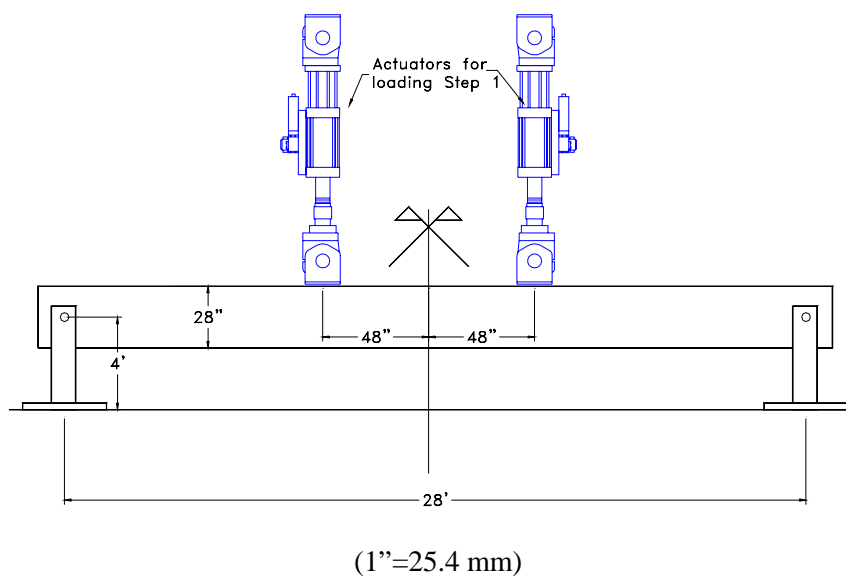
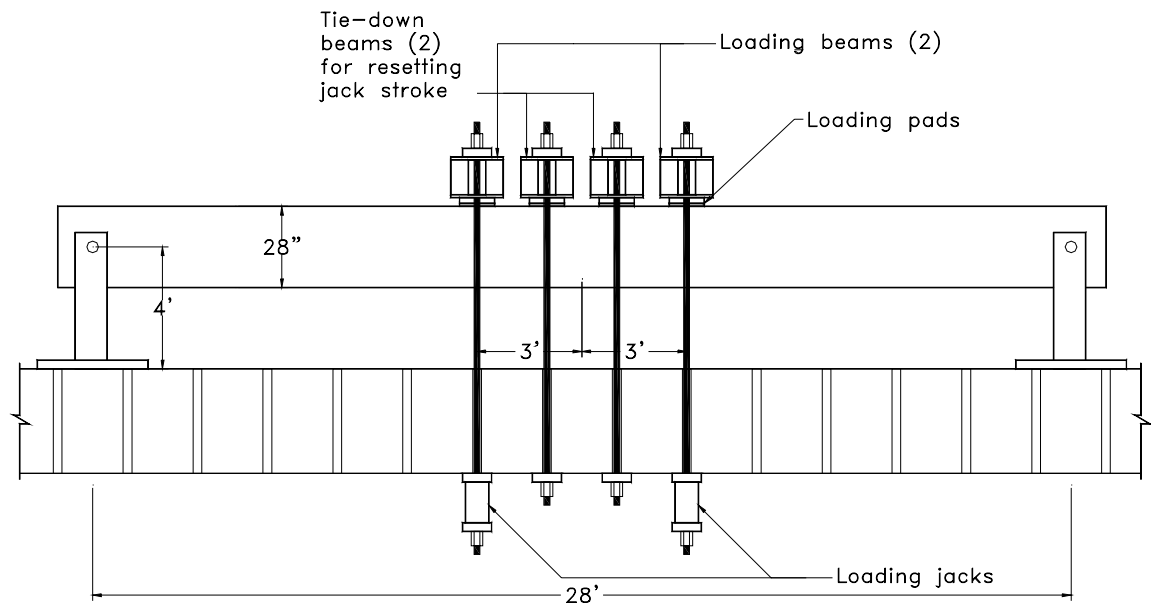
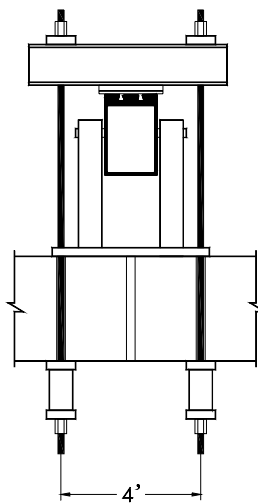


**Figure 3.1 Stiffness characterization of a hybrid girder**



(a) Elevation



(b) Side view

(1"=25.4 mm, 1'=305 mm)

**Figure 3.2 A schematic of the hybrid girder test setup**



**Figure 3.3 Test setup of the hybrid girder**

### **3.2 Test Observations**

During loading Step 1, a cracking noise was heard at a total load level of approximately 400 kN (90 kips). After unloading and reloading to that same level, no more noise was heard. However, when load was increased to 445 kN (100 kips), increased acoustic activity was noted. No visible damage to the specimen was observed.

During test Step 2, more acoustic activity was noted when load was ramped up to the target service load level. When the jacks are locked in place, no more acoustic activity was noticed. After 24 hours of sustained loading, the specimen showed very little change in stiffness. No visible damage was observed.

When loading continued, the girder remained linear-elastic up to failure. Bond failure (Figure 3.4) at splices of fabric (51 mm or 2" long) on the tension side of the specimen at mid-span was observed. No visible damage to the rest of the specimen was observed.



**Figure 3.4 Failure of the hybrid girder test**

### 3.3 Test Results

The load-displacement curve from test Step 1 is shown in Figure 3.5.

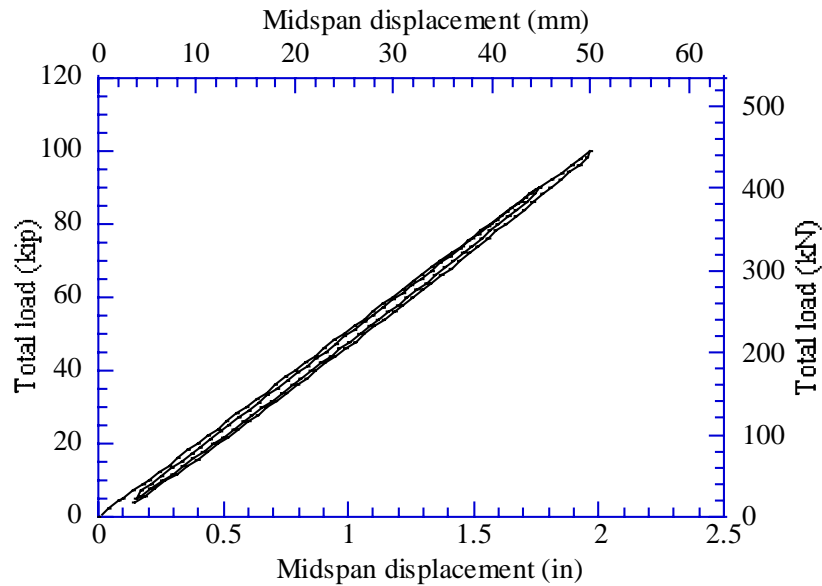


**Figure 3.5 Load-displacement relation of the hybrid girder under initial stiffness characterization**

The load-displacement curve of the test is shown in Figure 3.6. The unloading and reloading at a mid-span deflection of approximately 15 cm (6 inches) was induced during the resetting of the stroke in the jacks. Linear elastic behavior is observed. The displacement profile of the beam shows a well-behaved flexural system (see Figure 3.7). The longitudinal strain was measured at various locations in the girder. The load versus maximum strain curves, at midspan, are displayed in Figure 3.8 (tensile, bottom flange) and Figure 3.9 (compressive, top flange). A linear relationship up to failure is observed.

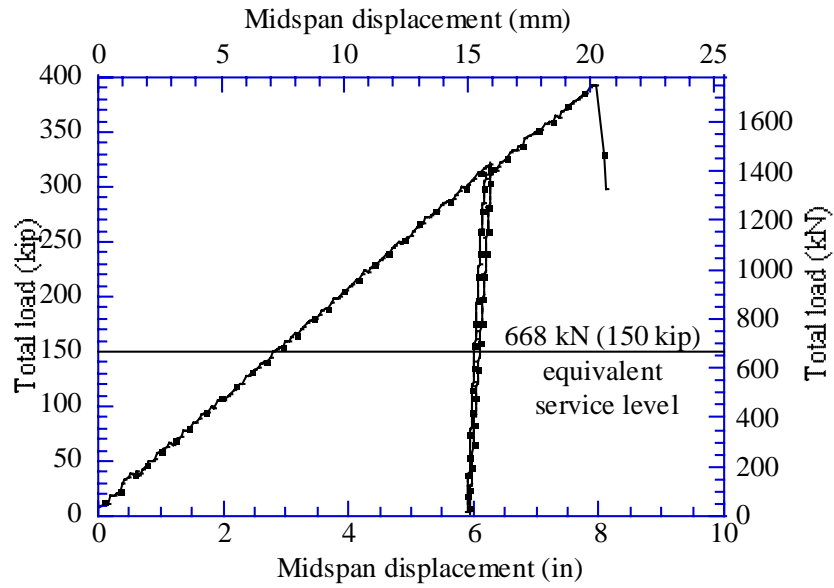


Figure 3.6 Load-displacement relation of the hybrid girder test

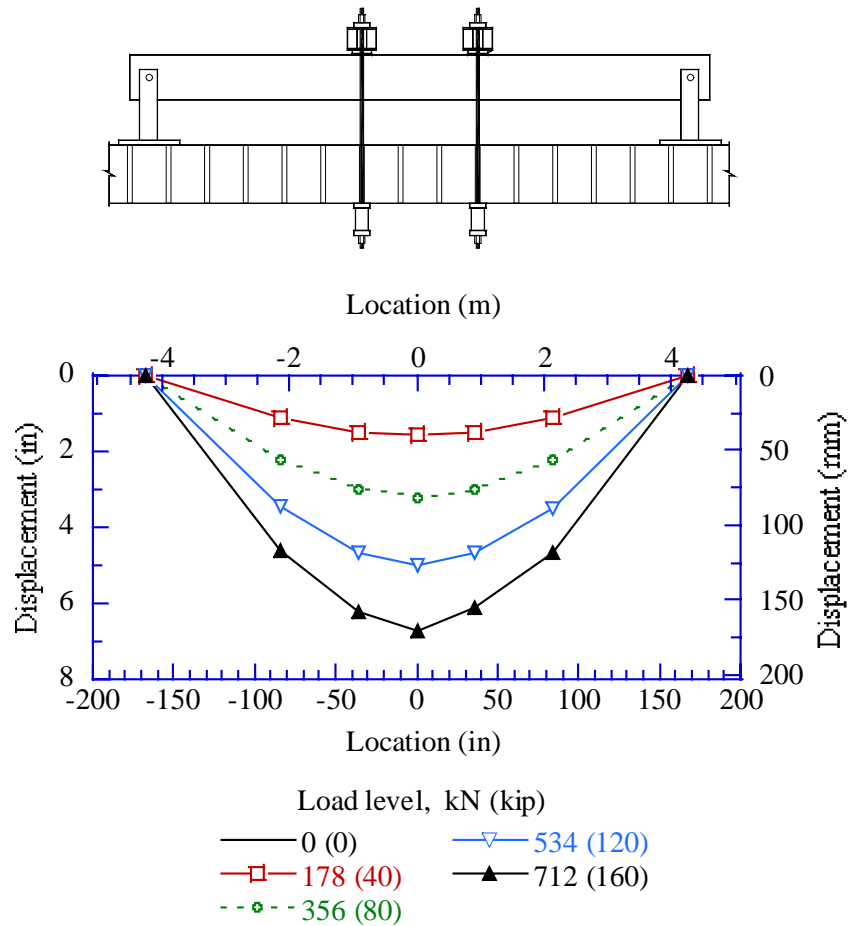
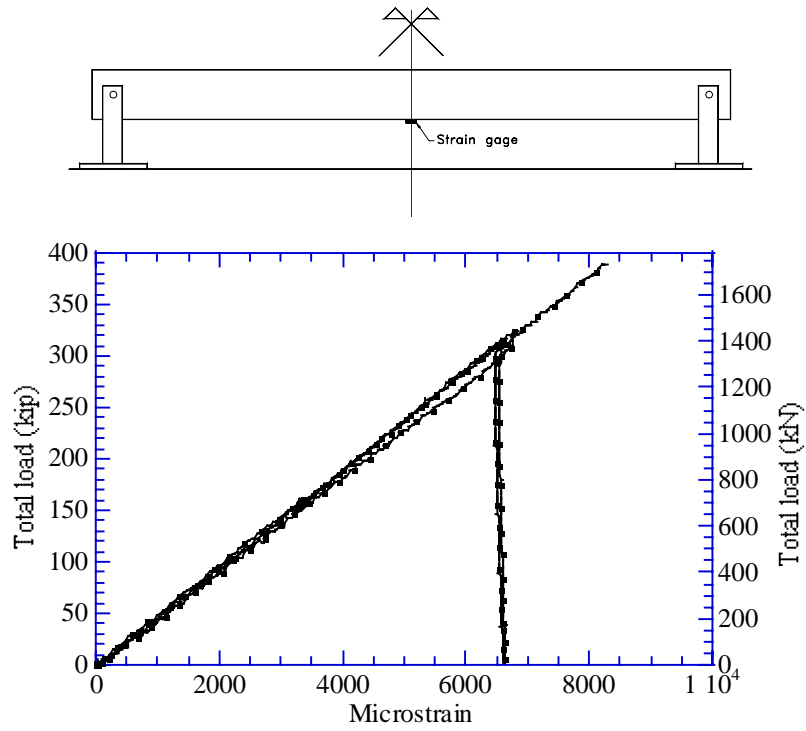
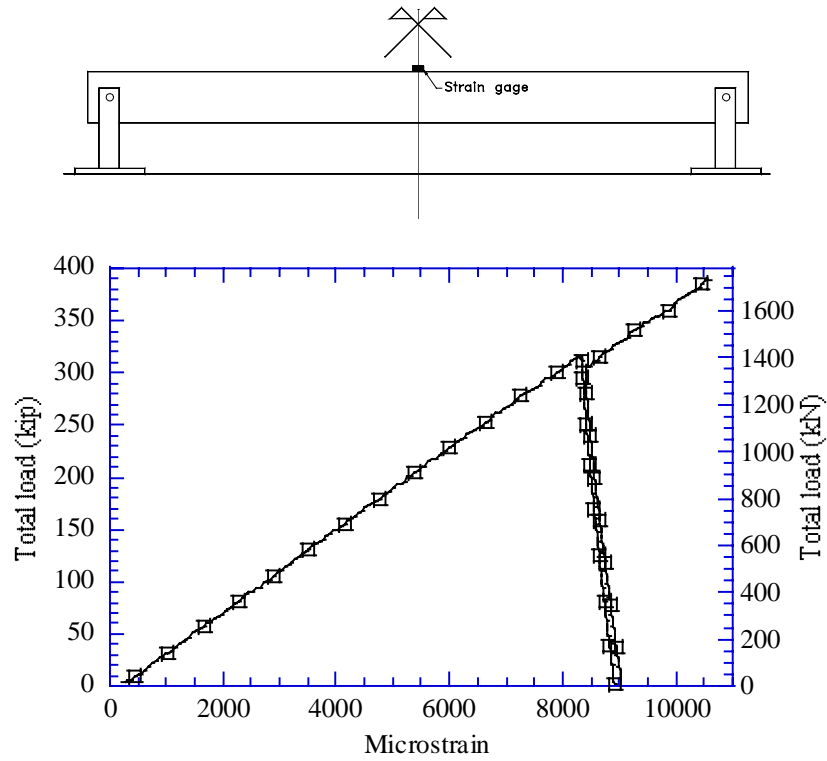


Figure 3.7 Displacement profile of the hybrid beam under four-point bending



**Figure 3.8 Load versus maximum longitudinal tensile strain at midspan**



**Figure 3.9 Load versus maximum longitudinal compressive strain at midspan**

The cross-sectional strain profiles at midspan can be seen in Figure 3.10. The neutral axis remains at the same location until failure.

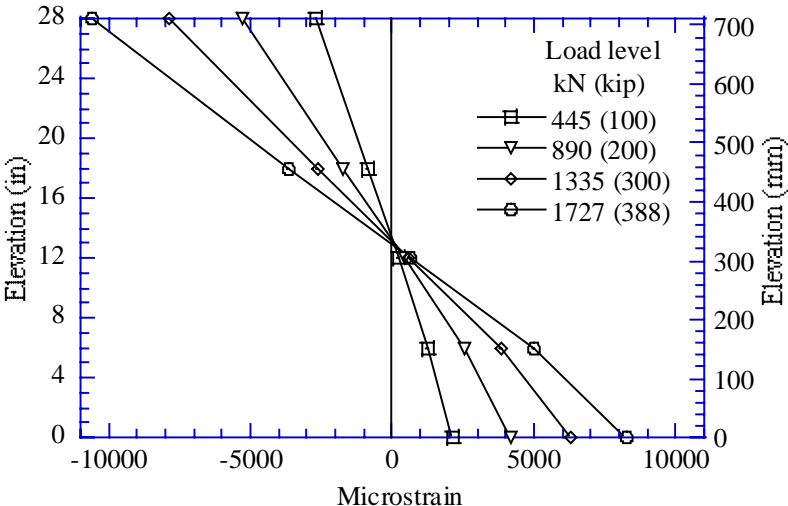


**Figure 3.10 Cross-sectional strain profile at midspan**

The shear strain was measured in both webs (locations 3 and 7) of the girder at section A, within the shear span, as shown in Figure 3.11. The curves also exhibit linear elastic behavior.

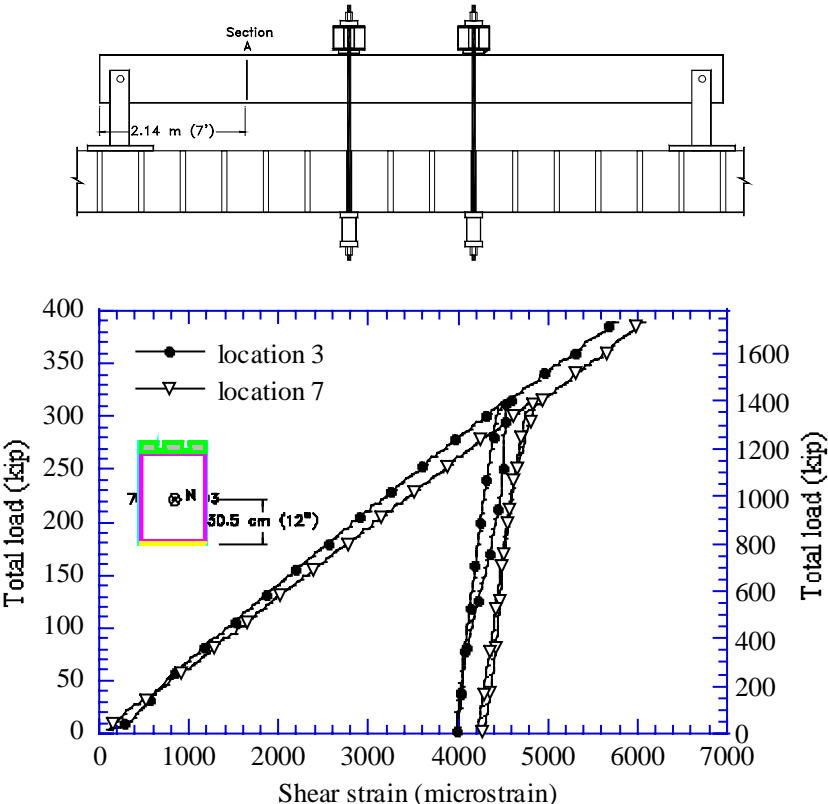


**Figure 3.11 Shear strain in the webs of the girder at Section A (within the shear span)**

After the test, the bottom section of the girder at midspan was cut and inspected. The unidirectional carbon layers were noted to have significant layer separation and splits, while the glass layers are undamaged (as shown in Figure 3.12).



**Figure 3.12 Section analysis shows delamination within the carbon layer**

## **4 TEST OF THE HYBRID TUBE SUBASSEMBLAGE**

### **4.1 Assembly and Construction of HTS Two-Girder Sub-Assemblage**

#### **4.1.1 Components**

The overall behavior of the Hybrid Tube System was evaluated by means of a flexure test and punching-shear tests on a two girder-deck subassemblage. The specimen consists of an arching deck spanning between two hybrid girders. The components, which include the two hybrid girders, the tension tie panels, and the shear connectors, are shown in Figure 4.1, Figure 4.2 and Figure 4.3 respectively.



**Figure 4.1 Specimen components: hybrid tube girders**



**Figure 4.2 Specimen components: tension tie panels**



**Figure 4.3 Carbon/epoxy stirrup snapped into girder anchorage cap**

#### **4.1.2 Assembly**

The construction of the two-girder/deck subassembly started with locally grouting steel pins through the ends of the girders. The end-hooks of the tension panels were temporarily placed in the grooves as shown in Figure 4.4. The tension panels are light enough for two people to carry and install (see Figure 4.5). The dowels were then snapped into the pockets in the top region of the girders as shown Figure 4.6.



**Figure 4.4** Placement of the end-hook of the tension panel in the groove



**Figure 4.5** Installation of the tension panels



**Figure 4.6 Installation of the dowels by snapping into the grooves**

A polyester resin mortar paste was poured into the grooves (shown in Figure 4.7). When pouring the groove, the end-hook of tension panel was lifted out of the groove and then inserted back into the mortar, which was partially squeezed out. A close-up taken after the grouting is shown in Figure 4.8. The resin mortar paste has a resin-to-sand weight ratio of 40:100. After the polymer concrete hardened, a concrete slab was cast on top of the specimen (Figure 4.9). Two different mix designs of concrete were used. One third of the slab used regular normal-weight concrete and the other two thirds used fiber-reinforced concrete (shown in Figure 4.27).



**Figure 4.7 Construction of the specimen: placement of stirrups into girders after snapping in tension tie panels**



**Figure 4.8 Construction of specimen: detail of connection after pouring polymer concrete**

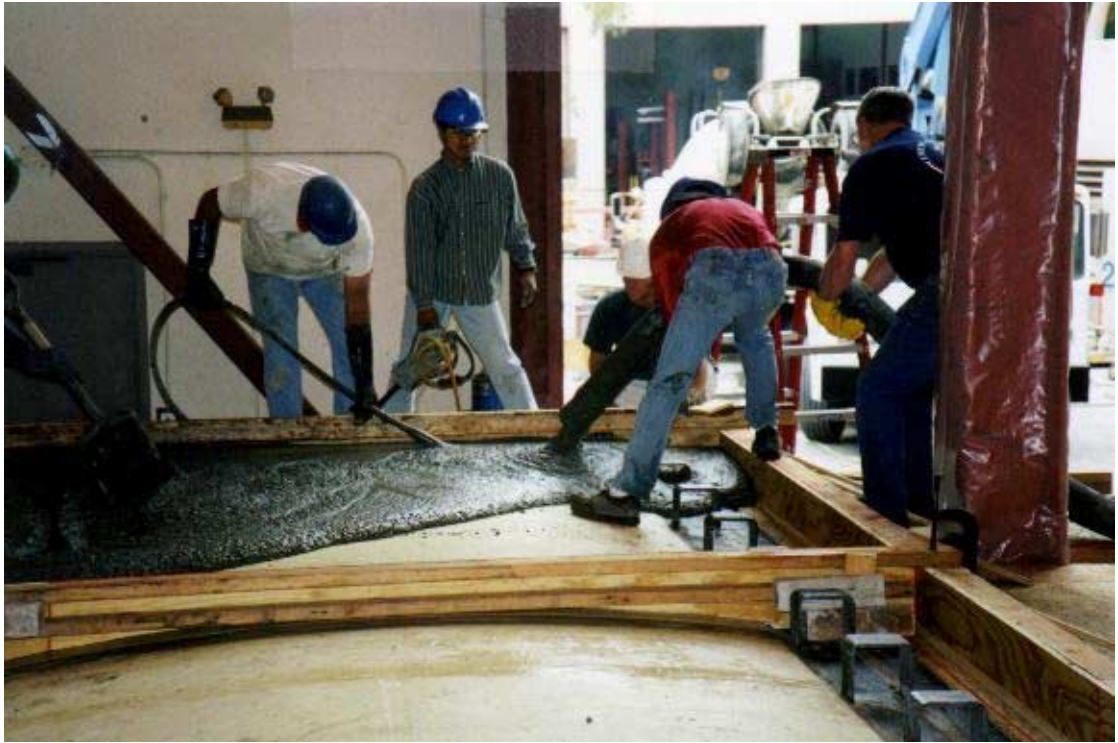


**Figure 4.9 Construction of Specimen: Casting Fiber Reinforced Concrete Deck**

## **4.2 Flexural Test**

### **4.2.1 Test setup**

The specimen was simply supported as shown in Figure 4.10 and Figure 4.11. Load was applied by two hydraulic actuators and distributed through four 20 cm x 51 cm (8" x 20") pads by means of rigid steel plates. The test setup layout and the specimen geometry are depicted in Figure 4.12 and Figure 4.13.

Load control was employed and the loading scheme consisted of 3 stages: 1) 3 cycles up to a total of 196 kN (44 kips) simulating service wheel loads with an impact factor; 2) 1 cycle up to a total of 334 kN (75 kip), simulating factored wheel loads and 3) 1 cycle up to a total of 668 kN (150 kip) simulating an equivalent system service load. The loading was to continued up to failure of the system.



**Figure 4.10 Test setup of the 2-girder subassemblage**



**Figure 4.11 Test setup and instrumentation of the 2-girder subassemblage**

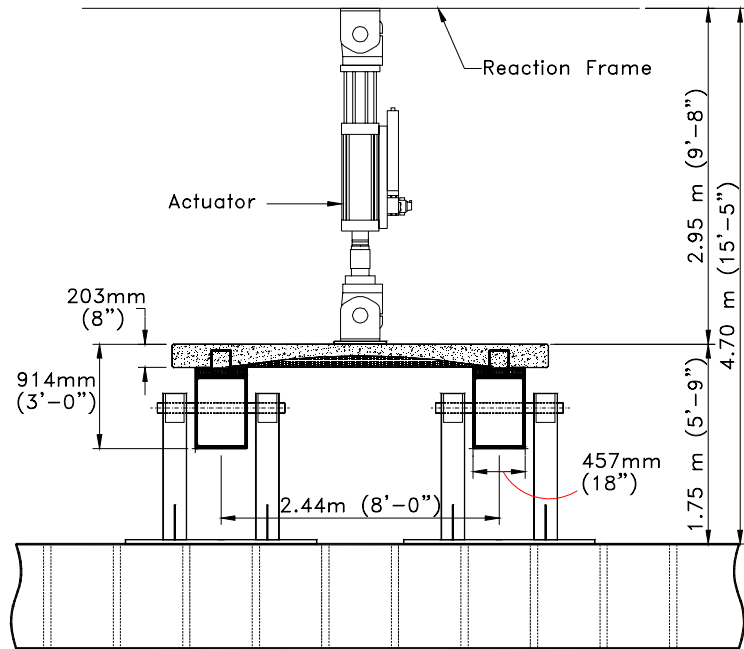
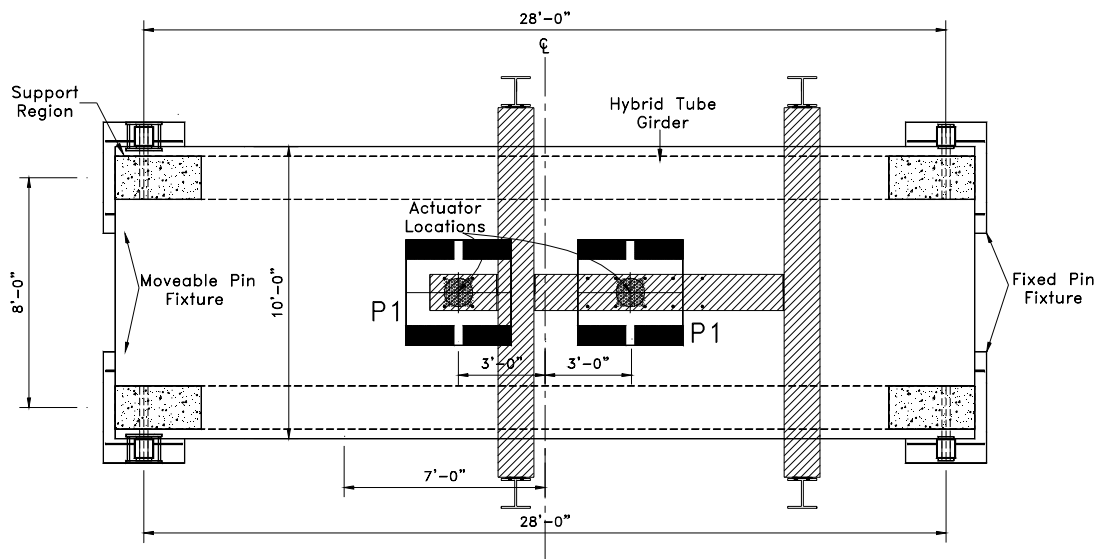


**Figure 4.12 Test setup of the 2-girder subassembly: cross-sectional view**



(1' = 305 mm, 1" = 25.4 mm)

**Figure 4.13 Test setup of the 2-girder subassembly: top view**

#### 4.2.2 Instrumentation layout

A total of 76 strain gages, 25 linear potentiometers and 4 rotation potentiometers were installed on the specimen, as shown in Figure 4.14.

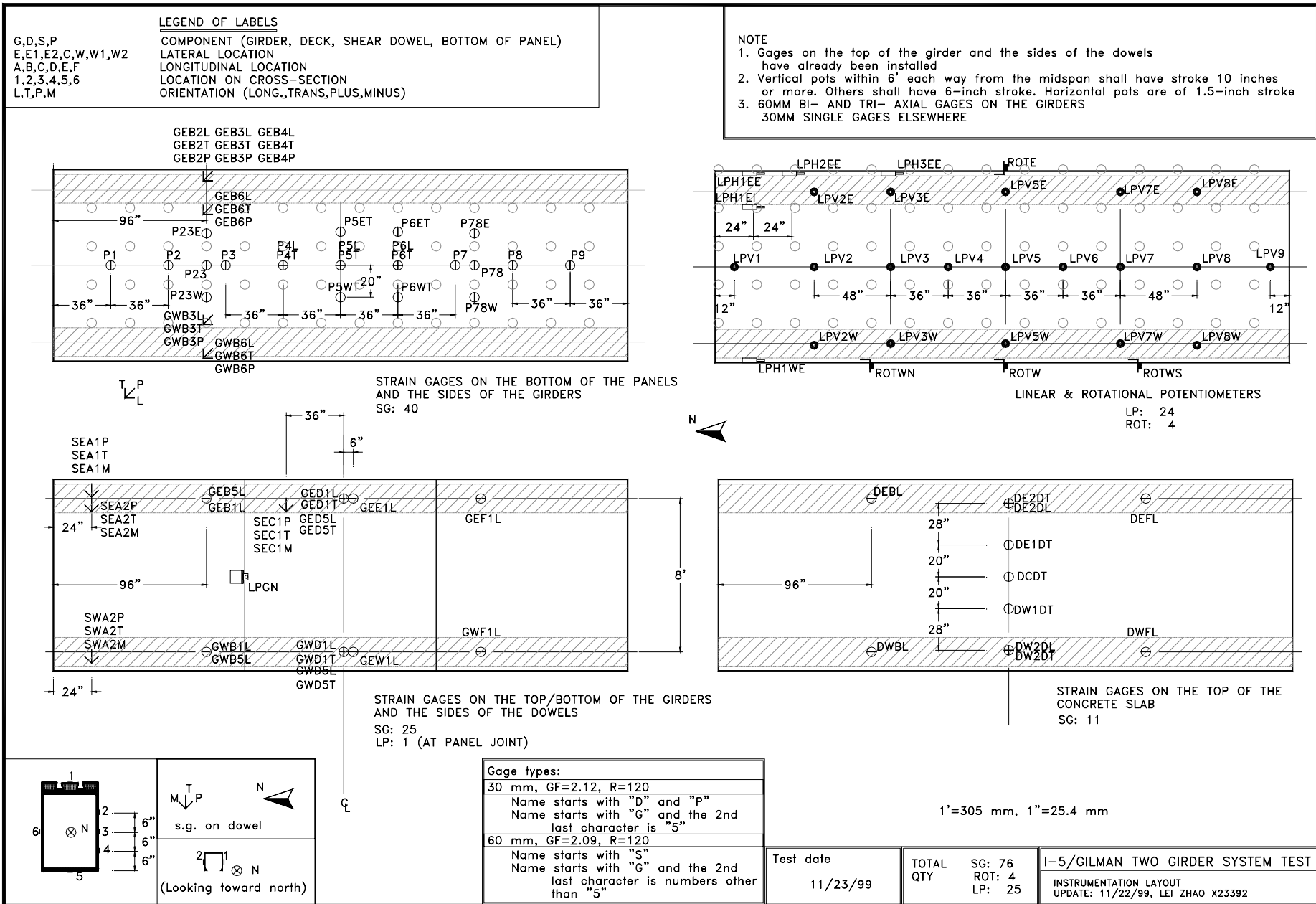


Figure 4.14 Instrumentation layout for the 2-girder sub-assembly

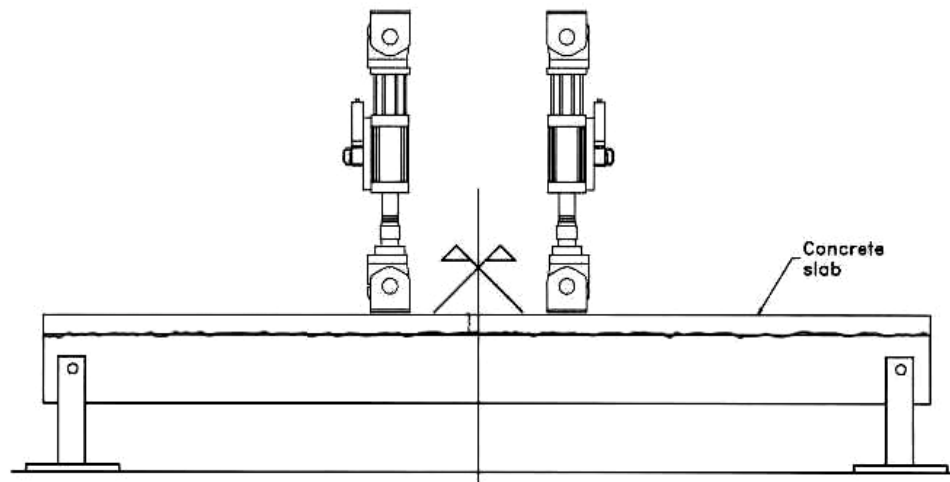
### 4.2.3 Test observations

The overall response was linear elastic during the first 3 load cycles up to 196 kN (44 kip) and no distress was observed in the specimen. For the next load cycle up to 334 kN (75 kip), no distress on the specimen was observed nor softening on the overall load versus displacement curves, but an audible noise related to crack was heard at a total load of 334 kN (75 kip). In the next load cycle, a crack developed longitudinally all along the interface panel/girders, as shown in Figure 4.15, at a load level of approximately 623 (140 kip), before the equivalent service load was attained. Slippage can be visually noted (see Figure 4.21) from the crack between the slab and the girders. At this point the system was unloaded and reloaded again all the way up to failure of the deck. In this last load cycle a stiffness degradation of more than 50 % was observed in the global response beyond the level of 623 kN (140 kips).

When approaching failure large-width longitudinal cracks developed at the top of the deck, close to the interface with the girder and around the load application region, as shown in Figure 4.16. The cracking noise intensified and transverse cracks also developed near the loaded area, followed by sinking of the steel plates into the panel. The deck failure took place at a total load level of about 220 kips.



(a) Photo showing separation between the concrete slab and the hybrid girder

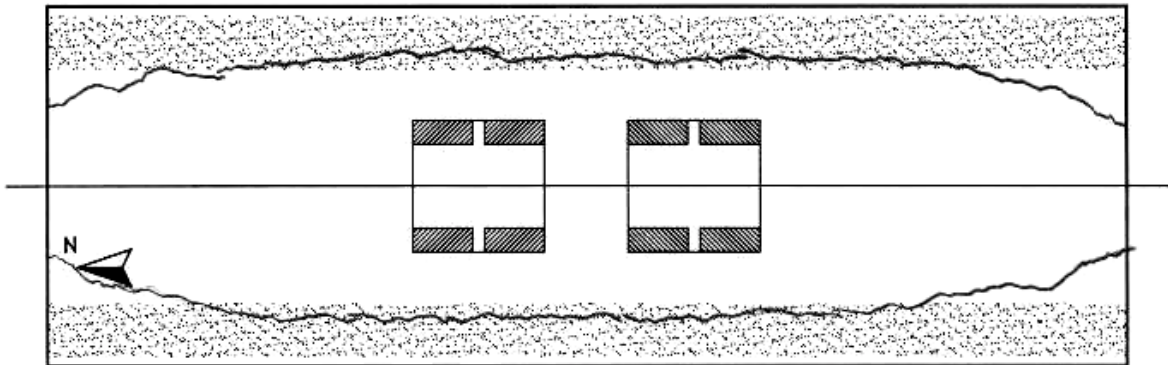


(b) Schematic of crack location

**Figure 4.15 Longitudinal Crack at Interface Deck/Girder**



(a) Photo showing longitudinal cracks in the slab



(b) Schematic of crack locations

**Figure 4.16 Failure mode: longitudinal crack in the slab**

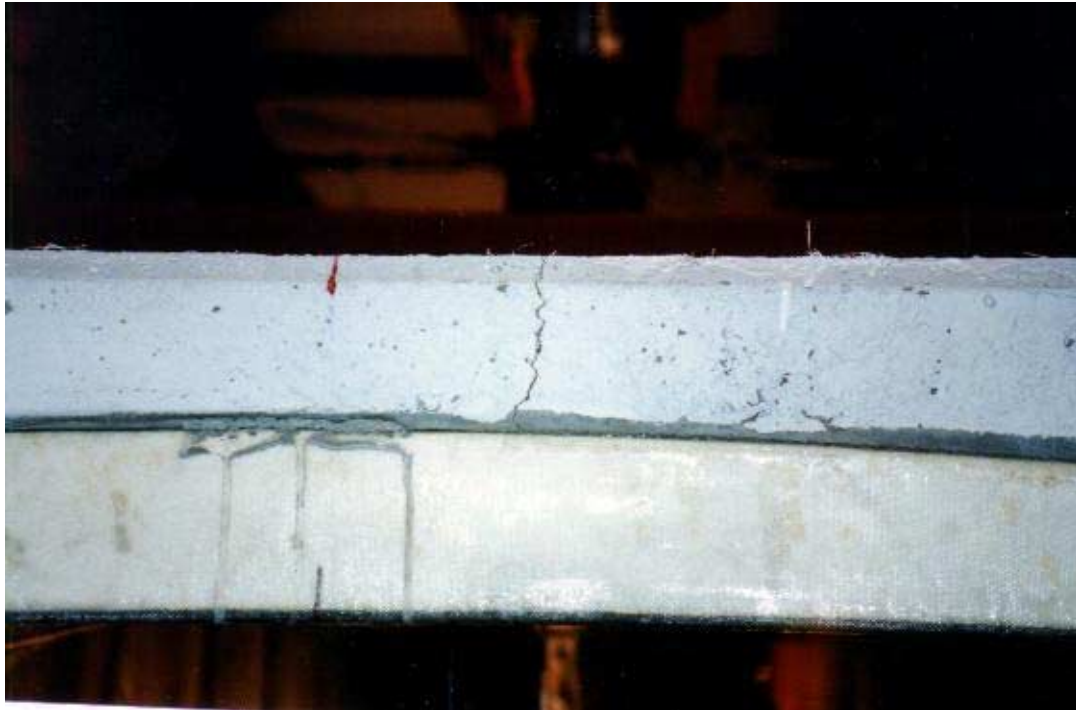


**Figure 4.17 Failure mode -- close-up**

#### 4.2.4 Test results

The total load versus mid-span displacement curves of the girders are shown in Figure 4.18; the curve of load versus central deflection of the panel is shown in Figure 4.19. The graph showing the total load versus slippage of the interface deck/girders is given in Figure 4.21.

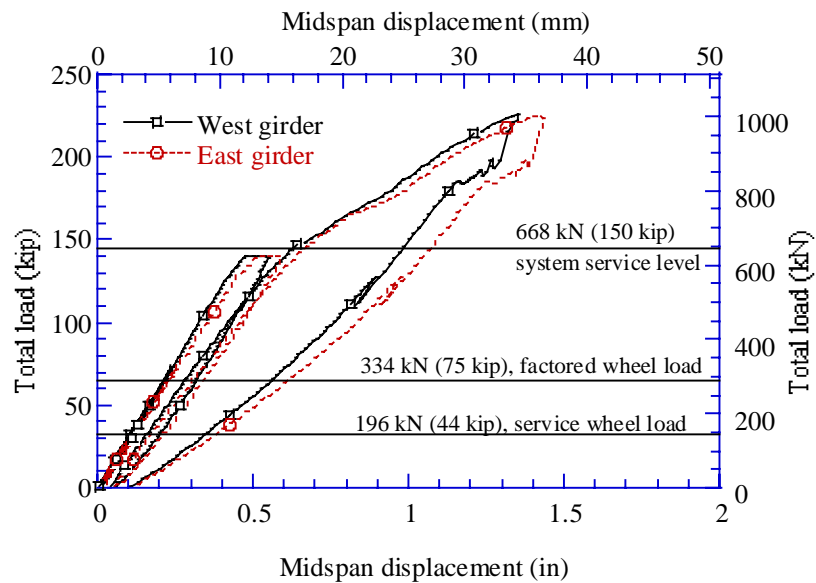
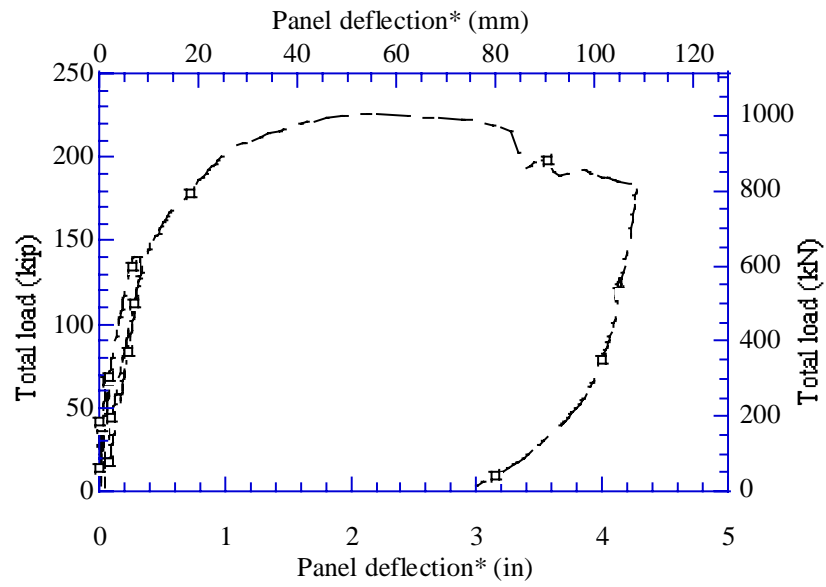


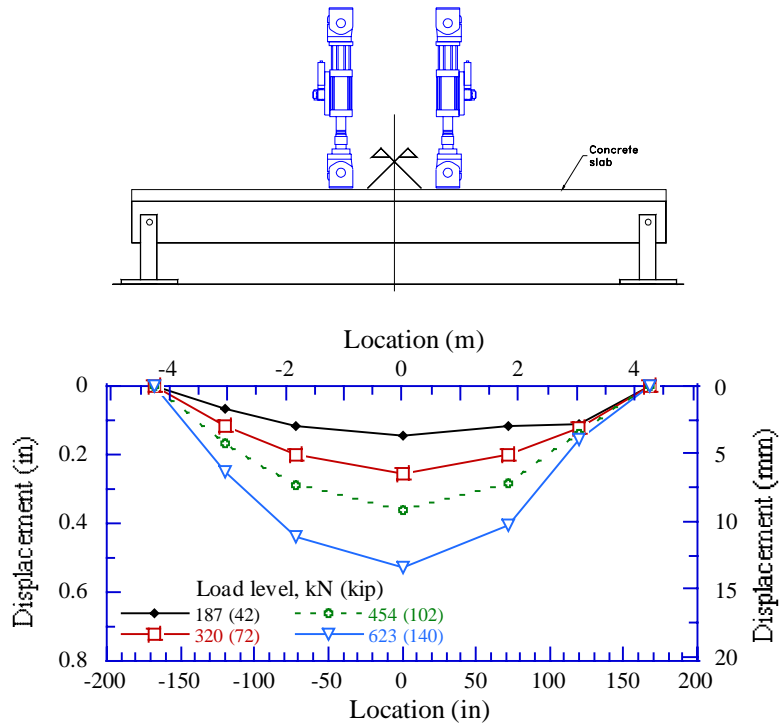
**Figure 4.18 Total load versus mid-span displacement of girders**



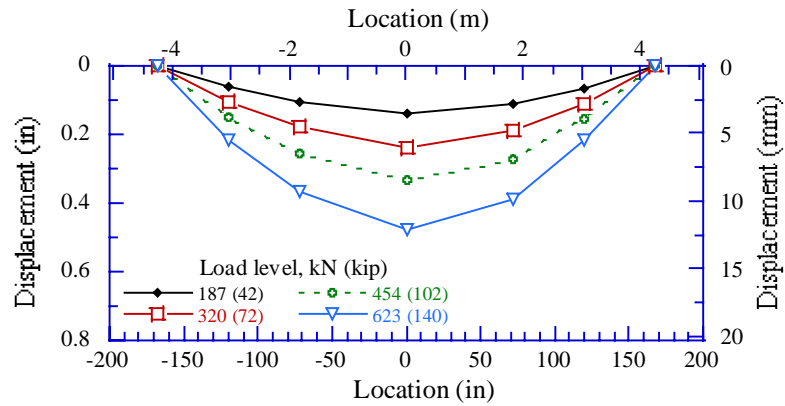
\* Calculated by subtracting the average girder displacement from total panel displacement at midspan.

**Figure 4.19 Total load versus central deflection of panel**

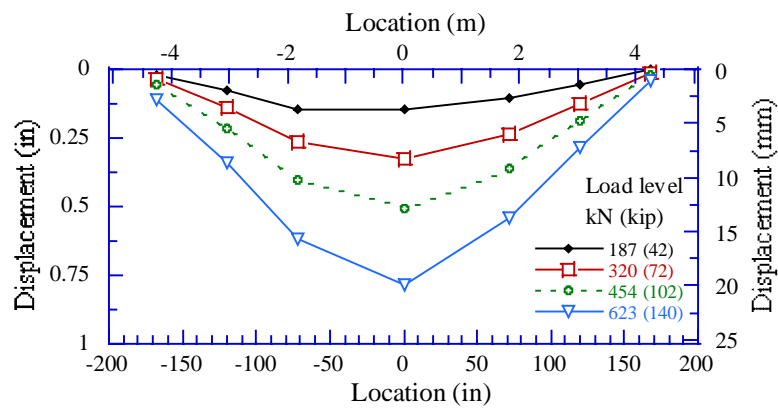
The vertical displacement profile of the girders and slab along the length of the subassembly, is shown in Figure 4.20 for increasing load levels. The subassembly behaves well in flexure.



(a) East girder



(b) West girder



(c) Center of slab

Figure 4.20 Displacement profile along the length of the subassembly

The slippage was measured at the interface between the slab and the girders. The four (lph1ee, lph1we, lph2ee and lph3ee) of these five measurements, which were taken on the exterior of the girder behaved similarly; and the one (lph1ei), which is recorded on the interior, behaved distinctively. This is caused by the fact that the tension panel has very low stiffness in the longitudinal direction of the system.

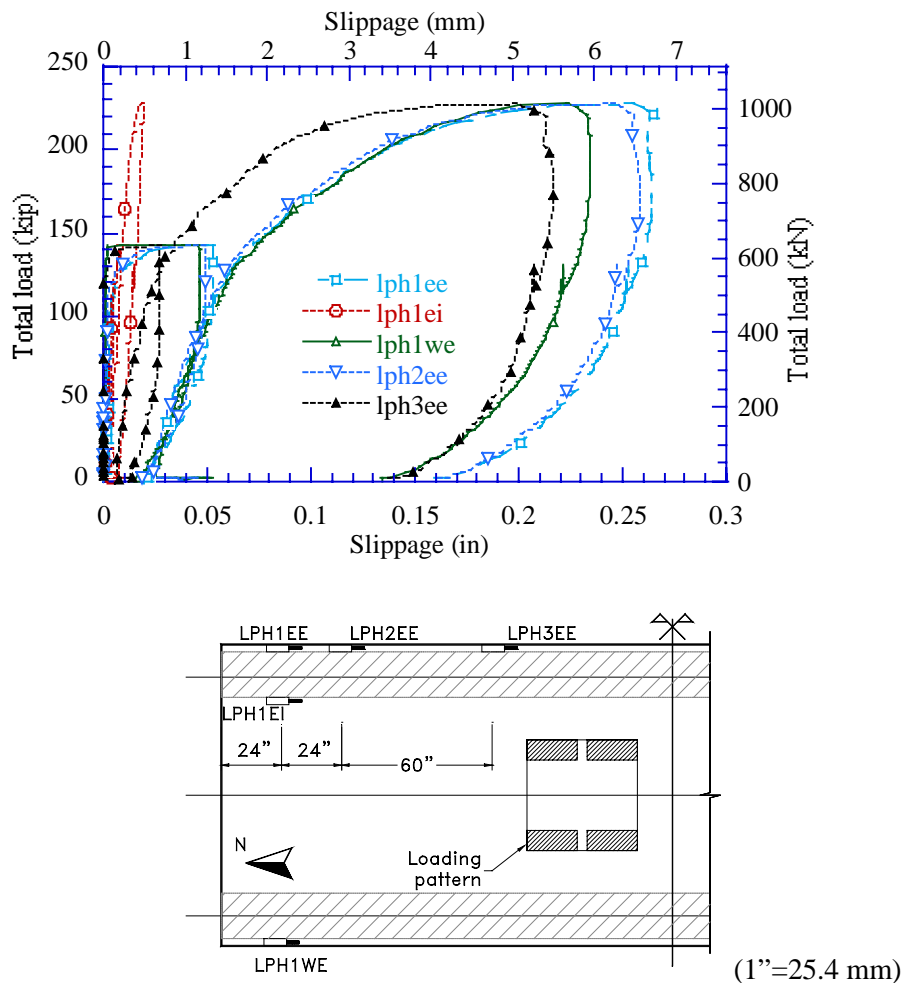


**Figure 4.21 Total Load versus Slippage at Interface Panel/Girder**

The total load versus longitudinal strain curve at the bottom of the East girder, at midspan, is given in Figure 4.22. A linear elastic behavior is also observed up to the load level of 623 kN (140 kips).

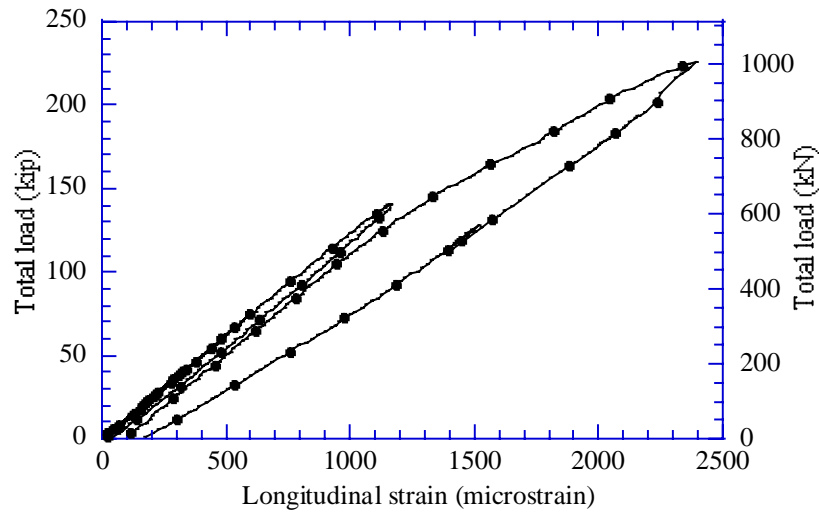


**Figure 4.22 Total load versus longitudinal tensile strain at midspan**

The longitudinal strain profile for increasing load levels is given in Figure 4.23 for the West girder and in Figure 4.24 for the East girder, at section B (2.44 m or 8' from the end of the specimen, see Figure 4.14). An approximately linear profile is observed showing a composite action between girder and slab in the linear elastic range of the system response before slippage took place.

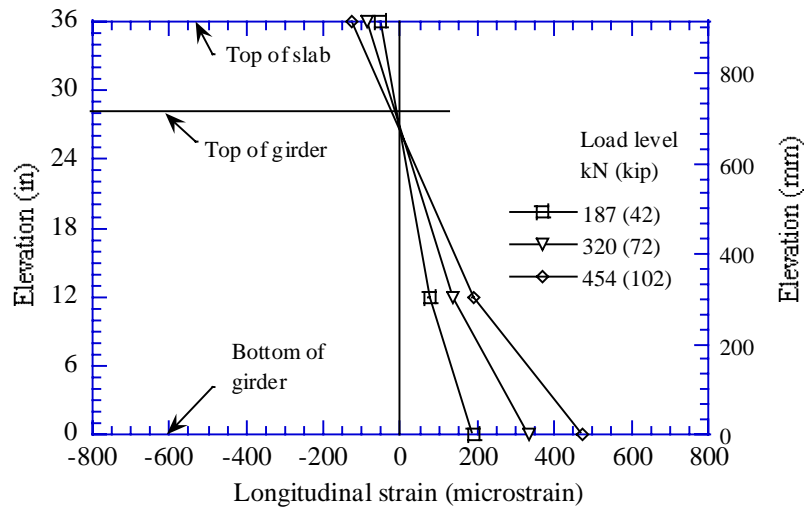


**Figure 4.23 Longitudinal strain profile at Section B of the west girder**

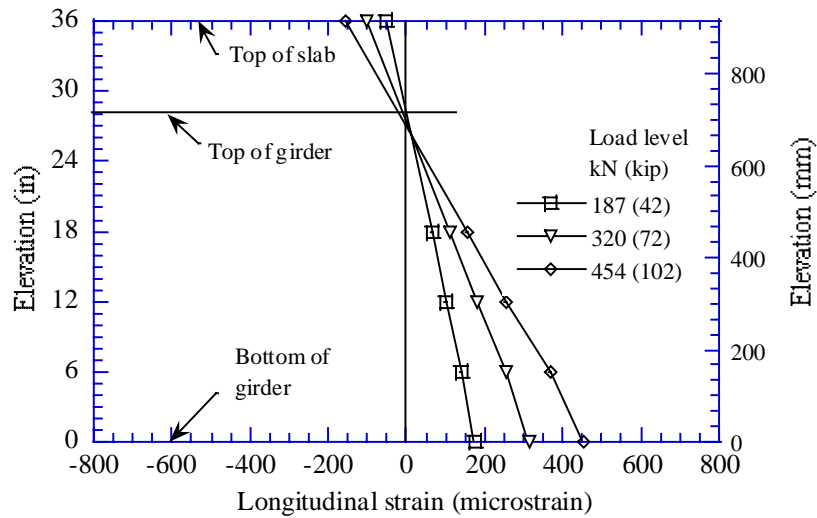


**Figure 4.24 Longitudinal strain profile at Section B of the east girder**

The shear strain in the shear dowels was also measured during the test. The total load versus shear strain curve is displayed in Figure 4.25 for a stirrup in the East girder near the support region (at 61 cm or 24” from the end of the specimen, see location A in Figure 4.14) and in Figure 4.26 for a stirrup near midspan (46 cm or 18” from midspan, see location C in Figure 4.14). It is observed that larger slips occurred near the support region, in the shear span of the girder, at the load level of 623 kN (140 kip).

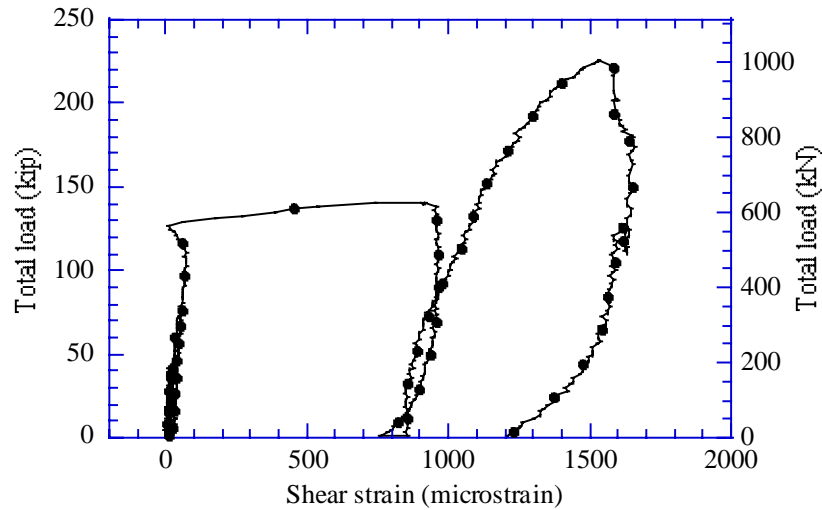


**Figure 4.25 Total load versus shear strain in stirrup near support**

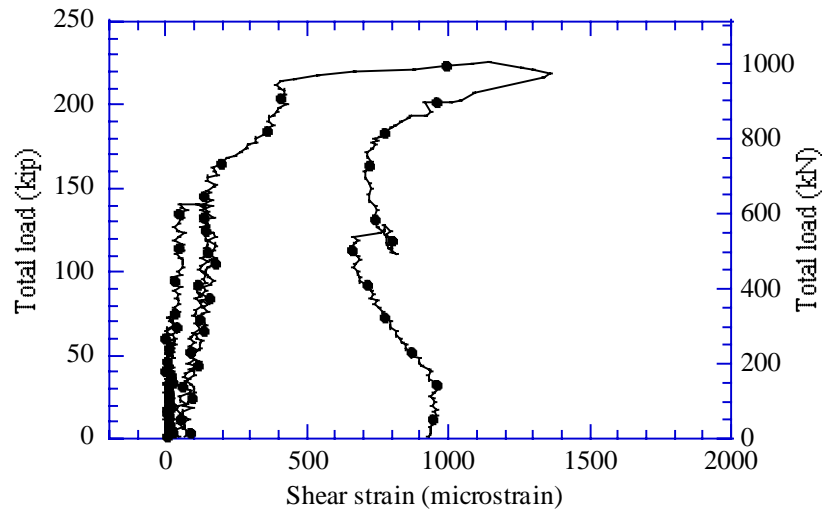


Figure 4.26 Total load versus shear strain in stirrup near midspan

### 4.3 Punching Shear Test

#### 4.3.1 Test setup

After the system test was completed, the specimen was vertically supported for the punching shear tests. One hole near each end of the specimen was core-drilled through the slab and the tension panel. Loads were applied with steel bars and jacks to the top of the specimen at those locations (shown in Figure 4.27). The 20 cm x 51 cm (8"x20") footprints of the loads was achieved by placing elastomeric pads. One of the loading locations is in the plain concrete part and the other is in the fiber-reinforced concrete part.

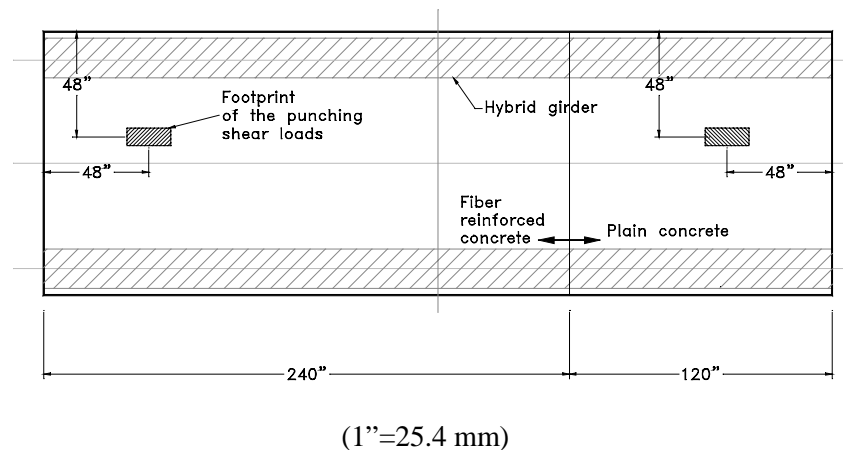


Figure 4.27 Locations of the punching shear loads

#### 4.3.2 Test observations

From the top of the slab, radial and tangential cracks developed at failure (Figure 4.28). The concrete slab separated from the tension panel (Figure 4.29).



**Figure 4.28 Failure mode: crack patterns on the top of the slab**

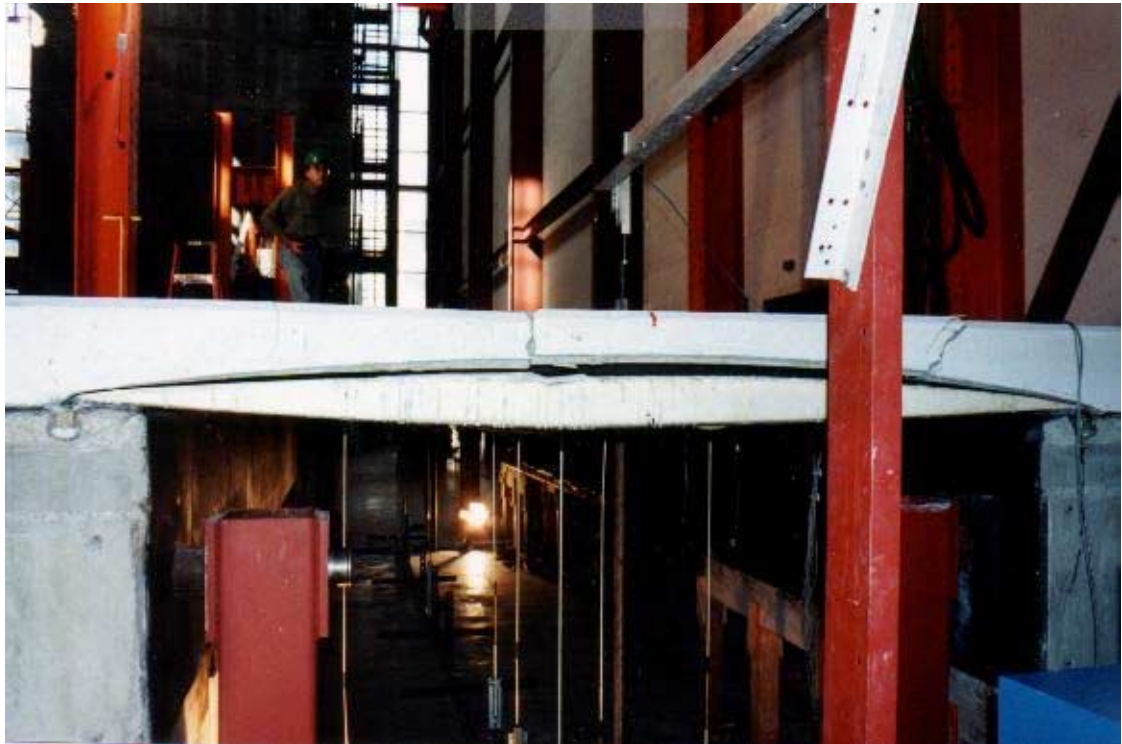


**Figure 4.29 Failure mode: separation between the slab and the tension panel**

### 4.3.3 Test results

The load versus displacement curves from both tests are graphically shown in Figure 4.30 and tabulated in Table 4.1. The addition of the polypropylene fibers results in a slightly higher punching shear capacity and less drop in load after the onset of failure.

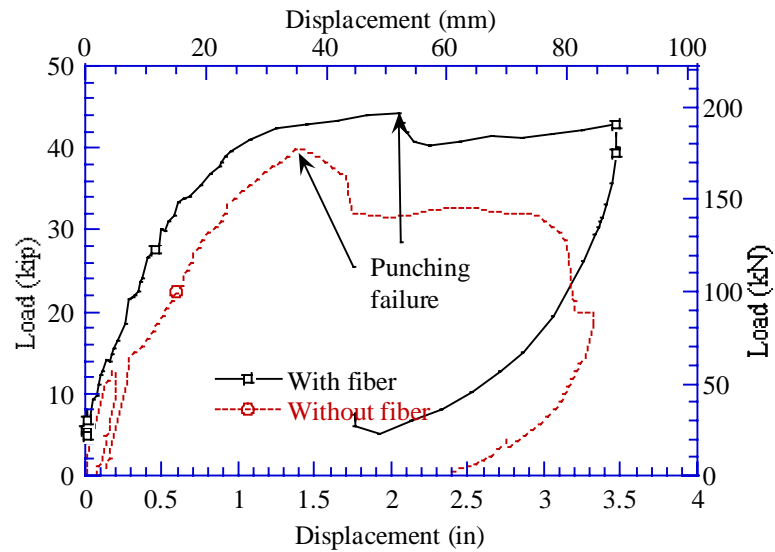


Figure 4.30 Load deflection curves of the punching shear test

**Table 4.1 Punching Shear Test Results**

Deck with fiber				Deck without fiber			
Load		Deflection		Load		Deflection	
kN	(kip)	mm	(in)	kN	(kip)	mm	(in)
0	0.00	0.0	0.00	0	0.0	0.0	0.00
20	4.41	0.2	0.01	21	4.7	1.3	0.05
28	6.27	0.6	0.02	31	6.9	2.0	0.08
41	9.32	1.2	0.05	49	10.9	3.3	0.13
54	12.24	2.5	0.10	57	12.8	5.2	0.20
66	14.89	4.5	0.18	71	15.9	9.5	0.38
82	18.51	6.5	0.26	96	21.6	14.3	0.56
96	21.60	7.3	0.29	109	24.4	16.7	0.66
105	23.54	9.1	0.36	122	27.4	18.2	0.72
119	26.66	10.4	0.41	136	30.5	22.2	0.87
134	30.19	12.7	0.50	150	33.8	24.8	0.98
148	33.30	15.4	0.61	166	37.3	30.4	1.20
164	36.83	20.6	0.81	179	40.2	35.3	1.39
177	39.69	24.1	0.95	173	38.8	38.7	1.52
191	42.91	36.7	1.44	163	36.6	43.2	1.70
193	43.35	41.7	1.64	152	34.1	43.8	1.73
197	44.24	51.9	2.04	140	31.6	49.6	1.95
186	41.84	53.4	2.10	146	32.7	64.8	2.55
181	40.67	62.2	2.45	142	31.9	69.9	2.75
186	41.75	77.5	3.05	137	30.7	76.8	3.02
188	42.23	82.6	3.25	121	27.2	80.2	3.16
191	42.88	87.7	3.45	97	21.8	81.0	3.19
191	42.95	88.1	3.47	89	19.9	84.3	3.32
189	42.41	88.1	3.47	82	18.5	84.4	3.32

## 5 CONCLUSIONS

In the preliminary characterization tests on components and subassemblages of the Hybrid Tube Modular advances composite bridge system have shown that while the bridge system overall exhibited the projected advantages of lightweight of the modular components, easy and fast assembly without heavy lifting equipment, and significant over-strength in the assembled system, other more local performance characteristics still need further improvement and development.

The individual hybrid tube test showed that not only significant capacity reserves over and above service or factored equivalent service load levels are present in the HTS girders but that failure did not occur until very large and clearly visible girder displacements were achieved. The overall response of the individual girder was essentially elastic all the way up to failure. The encountered failure mode at the maximum moment location by debonding of the short lap length in the glass fabric indicated that capacity increases are further possible by better detailing of the these laps.

The subassemblage of two HTS girders, the tension-tie form panels and the polypropylene fiber reinforced concrete deck showed that the modular system can lead to very fast erection times. In particular, the snap-in form panels and shear stirrups into the HTS girder grooves proved to be very simple. Mixing and handling issues with reduced slump and workability of the fiber reinforced concrete overlay need to be addressed and improved. Materials tests on the fiber reinforced concrete showed that the addition of 0.6% (by volume) of polypropylene fiber to the concrete mix did not change the actual concrete compression or tension capacities but rather the failure mode once initial failure onset had occurred. The benefit of the fibers was in the form of crack width control and with its better aggregate interlock characteristics once cracking was initiated.

The load test of the two-girder subassemblage showed that (1) horizontal shear transfer between the deck and the girders and (2) the stiffness and horizontal shear transfer between the deck and the form panels are critical issues which need to be improved. The horizontal shear force transfer between the concrete deck and girders failed by debonding along the entire girder length just slightly below the equivalent service load level calculated for the two girder test from the prototype bridge system. Subsequent to the horizontal debonding, the system capacity increased demonstrating the effectiveness of the snap-in carbon shear stirrups to load levels approaching 1.5 times the nominal service loads. While this may not be considered sufficient for actual design applications, the achieved horizontal shear capacities provide an important data point in the system development.

The horizontal shear failure (debonding) between the concrete deck and the girders unfortunately had a very negative effect on the concrete deck behavior. The design concept of arching action developing in the fiber reinforced concrete deck between girders held together via the form panel tension ties did not and could not materialize after debonding between the concrete deck and the HTS girders had occurred since the concrete deck could slide horizontally perpendicular to the girder line with only nominal constraints by the carbon shear stirrups which have very little stiffness in this direction. The sliding behavior between deck and girders resulted also in a separation between concrete deck and form panels, thus, preventing the development of monolithic flexural action in the transverse deck direction. In order to achieve monolithic flexural action between fiber reinforced deck and form panels, the panels need to be stiffer in flexure and in shear and mechanical bond between the form panels and the concrete overlay through ribs or rough spray or fiber mats needs to be established. A next generation of form panels with these improved characteristics is under development. Furthermore, the bond between the concrete deck and the HTS girders can be improved by transverse ribs at the girder top for mechanical interlock and by more snap-in shear stirrups. The same material quantities in the shear stirrups can be used for stirrups with half the original length and half the stirrup spacing which would result in improved shear transfer characteristics.

Finally, the punching shear test of deck sections with and without fiber reinforcement showed very little difference in punching shear response with only a slight post-punching response improvement in the fiber reinforced section due to better crack control. However, both punching shear tests clearly lacked the benefit of deck arching action due to the premature bond failure between deck and girder and punching shear failures occurred at load levels characteristic for decks with arching action. Again, significant improvements of punching shear characteristics can be expected with improved bond characteristics between concrete deck and form panels.

## 6 REFERENCES

---

- [1] Seible, F., Burgueño, R., Abdallah, M.G., et al, Advanced Composite Carbon Shell Systems for Bridge Columns under Seismic Loads, Proceedings from the National Seismic Conference on Bridges and Highways, San Diego, California, December, 1995.
- [2] Burgueño, R., Davol, A., and Seible, F., The Carbon Shell System for Modular Bridge Components, Second International Conference on Composites in Infrastructure, Tucson, Arizona, January 1998.
- [3] Zhao, L. and Karbhari, V., Lightweight Composite Deck Systems for Renewal, Engineering Mechanics: A Force for the 21 Century, ASCE 12<sup>th</sup> Engineering Mechanics Conference Proceedings, American Society of Civil Engineers, La Jolla, California, May 1998.
- [4] CHBDC, Canadian Highway Bridge Design Code – Section 16, Fibre-Reinforced Structures, final draft, July 6, 1996.
- [5] Seible, F., Hegemier, G. A., Karbhari, V. M., Davol, A., Burgueño, R., Wernli, M., and Zhao, L., The I-5/Gilman Advanced Composite Cable Stayed Bridge Study, University of California, San Diego, SSRP-96/05, 1996